Midbrain somatostatin-expressing cells control pain-suppression during defensive states

Nanci Winke[1,2§✉], Frank Aby[3§], Daniel Jercog[1,2§], Coline Riffault[1,2], Rabia Bouali-Benazzouz[3], Juliette Viellard[1,2,3], Delphine Girard[1,2], Zoé Grivet[3], Marc Landry[3], Laia Castell[4], Emmanuel Valjent[4,5], Stephane Valerio[1,2*], Pascal Fossat[3*] and Cyril Herry[1,2*✉]

[1]*Univ. Bordeaux, Neurocentre Magendie, U1215, 146 Rue Léo-Saignat, 33077 Bordeaux, France*

[2]*INSERM, Neurocentre Magendie, U1215, 146 Rue Léo-Saignat, 33077 Bordeaux, France.*

[3]*Interdisciplinary Institute for Neuroscience (IINS, CNRS UMR 5297), University of Bordeaux, Bordeaux Cedex, France.*

[4]*Université de Montpellier, Institut de génomique fonctionnelle (IGF), CNRS, Inserm, 141 rue de la Cardonille, 34094 Montpellier, France.*

[5]*INM, Univ. Montpellier, Inserm, F-34094 Montpellier, France.*

§ shared authorship
* shared seniority
✉ corresponding authors: nanci.winke@inserm.fr; cyril.herry@inserm.fr

Abstract

In threatening situations, animals exhibit a broad range of behavioral and autonomic responses. As such, a crucial adaptive response is the inhibition of pain, which facilitates relevant defensive behaviors that promote survival. Whereas the structures and mechanisms involved in fear and pain behaviors are well documented, little is known about the precise neuronal mechanisms mediating the emotional regulation of endogenous pain-suppression. Here, we used a combination of behavioral, anatomical, optogenetic, and electrophysiological approaches to investigate, in male mice, the role of somatostatin-expressing cells in the ventrolateral periaqueductal gray matter (SST^+ vlPAG cells) in the control of analgesia induced during defensive states. Our data indicate that optogenetic inhibition of SST^+ vlPAG

cells promotes analgesia irrespective of animal defensive state. In contrast, optogenetic activation of long-range SST$^+$ vlPAG cells that project to the rostral ventromedial medulla (RVM) abolishes the analgesia mediated by fear behavior. Together, these results identify a novel circuit mechanism composed of long-range SST$^+$ vlPAG cells projecting to the RVM that regulate analgesia elicited during defensive states.

Introduction

During threatening situations, the inhibition of pain is an essential adaptive response that can be crucial to promote self-preservation[1–4]. The inhibition of pain responses to a stimulus that would typically elicit pain is defined as analgesia[5]. In addition, previous studies have described that a fearful event can reduce pain sensitivity, a phenomenon referred to as fear-conditioned analgesia (FCA)[6]. In particular, pharmacological inactivation of the basolateral amygdala abolishes this fear-modulated analgesia and is associated with increased immediate-early gene c-Fos expression in the central amygdala and periaqueductal gray matter (PAG)[7]. The PAG is a midbrain structure that receives many cortical and subcortical inputs from brain structures involved in fear processing[8–11], projecting to the spinal cord primarily through a brainstem relay in the rostral ventromedial medulla (RVM)[12], a key structure involved in nociceptive transmission[13,14]. Indeed, the ventrolateral part of the PAG (vlPAG) is crucial for the descending control of pain[13,15] in the dorsal horn of the spinal cord (DH)[12], and several reports indicate that electrical stimulation of the vlPAG selectively inhibits responses to noxious stimuli in a variety of pain test conditions[12]. Moreover, analgesia induced upon vlPAG stimulation is opioid-dependent[16–18] and involves direct descending projections to the RVM and the DH[19–22] . Furthermore, previous research indicates that activation of the vlPAG induces analgesia through the recruitment of local GABAergic cells[23], which is

consistent with our understanding of the role of the GABAergic system in the descending control of pain[24,25]. Thus, the vlPAG is ideally positioned to mediate the emotional regulation of pain behavior, yet the underlying neuronal circuits and mechanisms are largely unknown. Here, we investigated the precise neural circuits within the vlPAG that mediate the suppression of pain behavior during threatening situations. We developed a unique behavioral paradigm where a cued-elicited defensive state promotes changes in pain sensitivity. Combining behavioral, anatomical, optogenetic, and electrophysiological approaches, we identified a novel midbrain to brainstem circuit mechanism composed of somatostatin positive (SST^+) vlPAG cells projecting to the RVM that is critically involved in the suppression of pain behavior during conditioned fear states.

Results

Cued-fear conditioning elicits analgesia

To evaluate the contribution of specific vlPAG cell populations to the fear modulation of pain behavior, we developed a novel cued fear-conditioned analgesia (CFCA) paradigm, consisting of a pain sensitivity assay during the presentation of threat-predicting cues (**Figure 1a**). In this paradigm, an initially neutral stimulus (the conditioned stimulus, CS^+) becomes associated with a footshock (the unconditioned stimulus, US), whereas another neutral stimulus serves as a control (CS^-). After conditioning, re-exposure to the CS^+ elicited freezing behavior, a behavioral readout of associative learned fear[26] (**Figure 1b and Supplementary Figure 1a**). Following the fear retrieval session, male mice were submitted to the pain sensitivity assay. Mice were placed on a Hot-Plate (HP) apparatus in which the floor plate temperature progressively increases while either CS^- or CS^+ were concomitantly presented. Plate temperature increased, and CSs were continuously played until mice displayed a nociceptive (NC) response reflecting pain behavior (**Figure 1c**),

78 defined by either jumping or hindpaw licking (**Figure 1d**). The detection of a NC response
79 terminated the test session (**see Methods**).

80 We observed a significant delay in the NC response performance for CS^+ compared to CS^-
81 presentations, reflecting that pain-suppression was selectively promoted by the threat-predicting
82 CS (**Figure 1e and Supplementary Figure 1b**). This increased NC latency during CS^+
83 presentation could alternatively be explained by a competition between freezing and pain-related
84 responses. However, freezing probability at the time of the NC response for CS^+ was remarkably
85 low and comparable to CS^- levels, suggesting that CS^+ increased NC response latency was not due
86 to competing freezing responses (**Figure 1f, see Methods**). Instead, these results suggest that fear
87 induced by CS^+ presentations drives the increase in NC latency. Importantly, such states induced
88 by our CFCA paradigm reflected fear associative processes (**Supplementary Figure 2**). To
89 demonstrate a causal link between cued-fear and analgesia, mice were submitted to an extinction
90 procedure to devalue the CS^+-US contingency and abolish the negative emotional state during CS^+
91 presentations (**Figure 1g**). Under these conditions, CS^+ presentation after extinction had no effects
92 on NC response latency (**Figure 1h**). Furthermore, the absence of auditory cues, or the presence of
93 auditory cues not associated with a threat, led to NC response latencies comparable to those
94 observed during CS^- presentations (**Figure 1i**). Finally, previous studies indicate that fear can lead
95 to vasoconstriction, which could result in a redirection of the blood flow to the skeletal musculature,
96 decreasing the temperature in the extremities of the body[27]. However, monitoring the back and tail
97 temperatures of mice submitted to the HP test did not reveal any differences between the CSs
98 presentations, suggesting that the increased latency was not due to fear-induced vasoconstriction
99 (**Supplementary Figure 1c-e)**. Overall, our results indicate that the presence of a conditioned
100 threat-predicting cue can selectively promote analgesia.

101

102 **Photostimulation of SST$^+$ vlPAG cells alters pain and fear behavior**

103 To identify the cell types in the vlPAG mediating the analgesic effect in the CFCA task, we
104 focused on GABAergic interneurons, whose activity is suggested to be inhibited during analgesia
105 through μ-opioid receptor-dependent mechanisms[12,25]. Using single-molecule fluorescent in situ
106 hybridization (smFISH, **see Methods**), we confirmed that the majority of vlPAG SST mRNAs
107 were expressed in inhibitory neurons (**Supplementary Figure 3**). As such, since somatostatin-
108 expressing interneurons (SST) are the most abundant interneuron class in the vlPAG[28], we focused
109 on this cell population. Thus, to evaluate the contribution of SST$^+$ vlPAG cells in CFCA, SST-Cre
110 mice were injected in the vlPAG with a Cre-dependent AAV expressing the Channelrhodopsin
111 (ChR2), Archaerhodopsin (ArchT), or GFP while optic fibers were bilaterally implanted targeting
112 this area (**Figure 2a, Supplementary Figure 11**). Next, mice were submitted to the CFCA task
113 while photostimulating SST$^+$ cells in the vlPAG (**Figure 2b**; **see Methods**). After fear retrieval
114 (**Figure 2c, e**; **Supplementary Figure 4a-d**), the optogenetic activation of SST$^+$ vlPAG cells
115 during the HP test had no effect on CS$^-$ presentation, whereas the same manipulation performed
116 during CS$^+$ blocked the increase in NC response latency compared to GFP controls (**Figure 2d and**
117 **Supplementary Figure 5a**). In contrast, optogenetic inhibition of SST$^+$ vlPAG cells increased NC
118 response latency for both CS$^-$ and CS$^+$ conditions compared to GFP controls (**Figure 2f and**
119 **Supplementary Figure 5b**). Importantly, these changes in NC response latencies were not due to
120 motor or aversive effects of the optogenetic manipulations, since photoactivation of SST$^+$ vlPAG
121 cells did not induce changes in distance traveled in an open field nor place aversion in a real-time
122 place preference test (**Supplementary Figure 5c-f**). In addition, we did not observe changes in
123 fear learning or expression when the footshock was replaced or paired with photoactivation of the
124 SST$^+$ vlPAG cells during the fear conditioning procedure (**Supplementary Figure 6**).

125 Altogether, these experiments confirmed that SST^+ vlPAG activation did not promote pain
126 responses and instead suggested that the SST^+ vlPAG cells are key elements of an endogenous
127 pain-suppression circuit. Additionally, the optogenetic effect observed during CFCA was not due
128 to alteration of somatostatin levels in our homozygous SST-Cre mice[29], as we observed the same
129 effect in heterozygous SST-Cre mice (**Supplementary Figure 7a-d**). Finally, in contrast with
130 STT^+ vlPAG cells, the optogenetic inhibition of another important class of vlPAG inhibitory cells
131 expressing the vasoactive intestinal peptide (VIP^+) did not change the NC response latencies during
132 CS^- or CS^+ presentations (**Supplementary Figure 7e-h, Supplementary Figure 10**).
133 Because our CFCA paradigm is dependent on fear associative processes (**Figure 1 and**
134 **Supplementary Figure 1-2**), it is possible that the optogenetic manipulation of SST^+ vlPAG cells
135 may have altered the expression of fear behavior. To control for this possibility, we optogenetically
136 activated or inhibited SST^+ vlPAG cells during a fear retrieval session following auditory fear
137 conditioning (**Figure 3a, b**). Our data indicate that whereas optogenetic inhibition of SST^+ vlPAG
138 cells had no effect on freezing behavior relative to GFP controls, their optogenetic activation
139 reduced freezing levels (**Figure 3c, d**). Altogether, our data show that the local SST^+ vlPAG
140 network can modulate both fear expression and the analgesia promoted during defensive states.
141

142 **Photostimulation of SST^+ vlPAG cells regulates spinal cord nociceptive transmission**

143 Consistent with our observations, previous studies found that the vlPAG is involved in fear-
144 conditioned analgesia[7]. It is conceivable that the SST^+ vlPAG cells are indeed part of a circuit
145 involved in the fear regulation of endogenous pain-suppression. To evaluate the effect of the
146 manipulation of SST^+ vlPAG cells on analgesia independently of the expression of fear behavior,
147 we evaluated the impact of SST^+ vlPAG cells manipulation on the control of nociceptive
148 transmission directly at the level of the spinal cord DH. Therefore, we performed extracellular local

149 field potential and single-unit recordings in the spinal cord DH during optogenetic stimulation of
150 SST^+ vlPAG cells in anesthetized mice (**Figure 4a**). Nociceptive stimulation induces early and late
151 neuronal responses at the level of the spinal cord DH[30] (A- comprising non-nociceptive Aβ and
152 nociceptive Aδ and C- fiber mediated, respectively; **Figure 4a**). While optogenetic activation of
153 SST^+ vlPAG cells during suprathreshold electrical stimulation of the paw increased the magnitude
154 of late nociceptive field potentials, the optogenetic inhibition reduced it (**Figure 4b, c**). To
155 determine whether this effect was specific to the nociceptive network, we recorded wide dynamic
156 range (WDR) cells in the DH, which receive both tactile (Aβ) and nociceptive (Aδ and C)
157 information[30]. We observed that photoactivation of SST^+ vlPAG cells increases both fast
158 nociceptive (Aδ-fiber) and slow nociceptive (C-fiber) responses without affecting non-nociceptive
159 (Aβ-fiber) responses (**Figure 4d**). Moreover, optogenetic inhibition of SST^+ vlPAG cells
160 specifically inhibited nociceptive responses, whereas non-nociceptive responses (Aβ-fiber)
161 remained unaffected (**Figure 4e**). In addition, we performed subliminal electrical stimulations that
162 did not elicit nociceptive neuronal responses. In this condition, we observed that removing
163 analgesia by activating SST^+ vlPAG cells elicited WDR responses at latencies corresponding to
164 nociceptive Aδ- and C-fibers (**Figure 4f**). Finally, the optogenetic activation of SST^+ vlPAG cells
165 had no effect on purely tactile fast latency spinal neurons (**Supplementary Figure 8**). Consistent
166 with our optogenetic manipulations during the CFCA task (**Figure 2**), these data suggest that, under
167 analgesia promoted by isoflurane, activation and inhibition of SST^+ vlPAG cells increased and
168 decreased nociceptive transmission, respectively, by specifically promoting pronociceptive and
169 antinociceptive responses in the spinal cord DH.
170

171 **SST$^+$ vlPAG-RVM-spinal cord pathway activation abolishes analgesia induced during**
172 **defensive states.**

173 We next evaluated whether SST$^+$ vlPAG cells mediate their analgesia modulation by contacting
174 WDR cells directly in the spinal cord or through the rostro ventromedial medulla (RVM), a
175 structure known to receive direct projections from vlPAG and mediate pain modulation[19,20] (**Figure**
176 **5a**). Anatomical tracing revealed large labeling of SST$^+$ fibers in RVM (**Figure 5b**) and only sparse
177 labeling within the spinal cord (SC; data not shown). By combining fluorogold retrolabeling from
178 the SC and GFP anterograde labeling from SST$^+$ vlPAG cells (**Figure 5c**), we observed RVM cells
179 projecting to the DH with close apposition of SST$^+$ putative boutons (**Figure 5d**), suggesting that
180 SST$^+$ vlPAG cells project to the RVM and contact DH-projecting RVM cells. Optogenetic
181 activation of SST descending fibers above the SC has no effect on WDR neural activity upon paw
182 electrical stimulation, suggesting that SST$^+$ vlPAG long-range projections to SC did not play a
183 major role in endogenous pain-suppression (**Figure 5e**). In contrast, photoactivation of SST$^+$
184 vlPAG inputs to the RVM increased both nociceptive (Aδ and C-fiber) responses (**Figure 5f,**
185 **Supplementary Figure 9**). Altogether, these data revealed that the SST$^+$ vlPAG-RVM-DH
186 pathway mediates endogenous pain-suppression.

187 We next addressed whether the SST$^+$ vlPAG-RVM-DH pathway was specific to mediating
188 endogenous pain-suppression induced by defensive states. Thus, SST-Cre mice were injected in
189 the vlPAG with a Cre-dependent AAV expressing the ChR2 or GFP, and a single optic fiber was
190 implanted above the RVM (**Figure 6a**). While photoactivation of the SST$^+$ vlPAG-RVM pathway
191 promoted nociception (**Figure 5f**), it did not impact fear expression as freezing levels remained
192 unchanged (**Figure 6b**). Consistently, activation of the SST$^+$ vlPAG-RVM pathway during CFCA
193 had no impact on CS$^-$ presentation, whereas the same manipulation performed during CS$^+$ blocked

194 the increase in NC response latency compared to GFP controls (**Figure 6c, d**). Overall, these data
195 suggest the existence of two populations of SST^+ vlPAG cells mediating fear expression and
196 analgesia induced by defensive states. (**Figure 6e**). Altogether, our results indicate that the SST^+
197 vlPAG-RVM-DH pathway is critically involved in the analgesia induced during defensive states.
198

199 ## Discussion

200 In this study, we established that SST^+ vlPAG cells control analgesia during defensive states in
201 male mice. Endogenous pain-suppression was mediated by long-range SST^+ vlPAG cells
202 projecting to the RVM, which, in turn, transmitted the pain signal to the DH of the spinal cord
203 (**Figures 2 and 5**). Finally, our data indicated that SST^+ vlPAG cells can regulate both fear
204 expression and the analgesia promoted during defensive states, and that the expression of these two
205 behaviors can be segregated by precisely targeting the SST^+ vlPAG-RVM pathway (**Figure 6**).
206 Together, these results identify a novel midbrain to brainstem circuit mechanism composed of long-
207 range SST^+ vlPAG cells projecting to the RVM that regulate analgesia elicited during defensive
208 states. Pain mechanisms and their modulation are known to exhibit sex-dependent differences[31],
209 and thus we cannot exclude the possibility that the circuits described here may differ in females.
210 Nevertheless, recent studies of RVM-spinal cord descending control suggest broadly similar
211 organization and function across sexes[32,33]. Direct experimental investigation in female animals
212 will be required to determine the extent to which the present findings generalize across sexes.

213 Our observations of the involvement of vlPAG in our cued-based fear conditioned analgesia
214 paradigm are consistent with previous studies of contextual-based FCA involving this region[7]. In
215 such FCA studies[6], animals undergo contextual fear conditioning followed by pain behavior testing
216 in the same conditioning context, thereby limiting the temporally precise elicitation of aversive

217 states. Instead, our behavioral paradigm goes beyond these limitations by promoting defensive
218 states through a cued conditioned stimulus, advancing toward temporally specific manipulations
219 such as optogenetics, and allowing us to study the phenomena with a within-subject experimental
220 design through subsequent $CS^{+/-}$ presentations. Nevertheless, since the circuits involved in
221 contextual and cued fear may differ[30,34], this might also imply different circuits involved in the
222 emotional modulation of pain-suppression behavior. To our knowledge, this is the first
223 demonstration of a cued fear-conditioned analgesia model in rodents. Addressing potential
224 differences in the circuitry involved in contextual and cued fear-induced analgesia will require
225 further investigation.

226 Our observation that photoactivation of SST^+ vlPAG cells not only abolished analgesia during
227 defensive states but also decreased freezing expression has far-reaching functional consequences.
228 Two independent previous studies found that long-range inhibitory inputs from the central medial
229 amygdala contact inhibitory cells within the vlPAG, implicated in different roles: the modulation
230 of fear behavior[23] and nociceptive transmission[35]. Notably, both studies describe the involvement
231 of vlPAG inhibitory cells in a disinhibitory circuit mechanism of long-range projecting excitatory
232 cells as the underlying neural substrates responsible for such modulations[23,35]. We observed that
233 SST^+ cells are the most abundant inhibitory cell type in the vlPAG (**Supplementary Figure 3**).
234 Thus, it is conceivable that the SST^+ vlPAG cells are indeed part of a circuit involved in the
235 emotional regulation of endogenous pain-suppression. Notably, global manipulation of SST^+
236 vlPAG cells cannot disentangle their role in analgesia and fear behavior at the local level (**Figures
237 2 and 3**). Because the studies mentioned above exclusively addressed the contribution of vlPAG
238 circuits to either pain[35] or fear[23] behavior, these studies may have been oblivious to alternative
239 behavioral readout interpretations. Here, we demonstrated that SST^+ vlPAG cells projecting to the
240 RVM modulate analgesia induced during defensive states without impacting the behavioral

241 expression of fear (**Figure 6**). Thus, our results suggest that fear and analgesia signals rely on
242 overlapping neuronal circuits and that the discrimination between these two states could be
243 mediated within the vlPAG network. Altogether, our data are consistent with the existence of
244 different populations of SST^+ cells within the vlPAG that mediate fear behavior and analgesic
245 information, defined by their output connectivity.

246 The lateral inhibition model of analgesia within the PAG relies on the activation of PAG
247 excitatory cells projecting to the RVM. More precisely, in this model, analgesia is thought to occur
248 through an opioid-dependent inhibition of GABAergic cells, ultimately disinhibiting excitatory
249 cells projecting to the RVM[12,20,21]. Our data indicate that, in addition to this disinhibitory
250 mechanism, analgesia is also mediated by the inhibition of a direct long-range SST^+ neurons
251 projection onto RVM cells projecting to the DH (**Figure 6**). In line with this, inhibition of vlPAG
252 SST cells induced analgesia in our experiments, consistent with previous findings obtained using
253 chemogenetic approaches[36]. However, important differences emerge when comparing our results
254 with Zhang et al.[34]. In that study, activation of vlPAG SST cells produced hyperalgesia, whereas
255 in our study, activation of SST^+ vlPAG cells did not induce hyperalgesia but instead suppressed
256 fear-conditioned analgesia. One key distinction between the two studies is the experimental
257 context: Zhang et al. examined this circuit in a neuropathic pain model, whereas our work focuses
258 on acute nociceptive processing and fear-dependent modulation of pain. Thus, the functional
259 contribution of SST^+ vlPAG cells may depend on the behavioral and pathological state, with
260 potentially distinct roles in chronic versus acute pain conditions[35]. In addition, methodological
261 differences, such as our nociceptive test that uses a slow temperature ramp, may impose a floor
262 effect that limits the detection of thermal hyperalgesia. Our results are therefore consistent with the
263 parallel inhibition-excitation model, in which inhibitory and excitatory cells form two distinct,
264 parallel descending pathways for pain modulation[24]. Indeed, previous studies have identified

265 inhibitory projections within the PAG–RVM-spinal cord dorsal horn neuraxis[37], and our results
266 suggest that SST$^+$ vlPAG cells contribute to analgesia within this broader framework. At the same
267 time, our data indicate that vlPAG SST$^+$ cells are not exclusively inhibitory, as approximately one
268 third co-localize with excitatory markers, and recent work has shown that excitatory SST$^+$ vlPAG
269 cells project to the RVM[36]. Together, these observations raise the possibility that distinct SST$^+$
270 subpopulations contribute differently to descending pain control, with long-range vlPAG SST$^+$
271 cells participating in the excitatory pathway projecting throughout the PAG–RVM-spinal cord
272 dorsal horn neuraxis, and local GABAergic vlPAG SST$^+$ cells contributing to local circuit
273 dynamics related to fear response, such as freezing[23]. We identified a novel midbrain to brainstem
274 circuit mechanism composed of SST$^+$ vlPAG cells that project to the RVM, thereby regulating
275 analgesia during defensive states. Substantial progress has been made in outlining the midbrain
276 circuitry of the endogenous pain-suppression pathway[12,24,26]. However, only more recently have
277 high cortical areas been shown to be involved in analgesia[7,38]. Previous reports describe
278 connections between CeL and vlPAG inhibitory neurons in the modulation of pain behavior[35,39].
279 Future work is required to elucidate whether the exact circuit that regulates analgesia is mediated
280 by different negative emotional states, such as fear, depression, or stress.

281 Recent human reports reveal strong comorbidity between mood and anxiety disorders with and
282 pain-related disorders[40], suggesting that the deregulation of the circuits mediating the interplay
283 between emotional and pain behavior could be at the core of such psychiatric conditions.
284 Comprehensive knowledge about the circuits mediating the emotional regulation of pain behavior
285 is urgently needed. We identified an SST$^+$ cell type- and pathway- specific involvement in the
286 mechanisms that mediate the emotion-dependent regulation of pain behavior. Thus, these findings
287 may empower the development of more effective analgesic therapies by the improvement of further
288 refined pharmacological targets.

289

290 ## Figure Legends

291 **Figure 1. Fear modulation of pain behavior. a.** Schematic of the setup and the CFCA paradigm.
292 The paradigm consists of a discriminative auditory fear conditioning test followed by a pain
293 sensitivity assay (for details, see Methods). **b.** Average freezing values for CS^+ were higher than
294 CS^- or baseline (BL) periods during retrieval (****, $P < 0.0001$, one-way RM ANOVA, n = 12
295 mice). **c.** Example of the infrared digital thermographic camera view of a mouse during the FC HP
296 test. After 1 min of context acclimatization, the plate temperature steadily increases at 6 ºC per min
297 (HP start). CSs started 130 s after the HP start and continued until mice displayed an NC response
298 (licking the hindpaw or jumping). **d.** Example of assessed hindpaw licking NC response. **e.** Latency
299 of NC response on the FC HP test increased during CS^+ compared to CS^- (***, $P = 0.0005$,
300 Wilcoxon matched-pairs signed rank test, n = 12 mice). **f. Left**: dynamics of freezing probability
301 at CS onset and NC response for both CS^- and CS^+ (freezing periods for each individual mouse are
302 displayed by rows in grey; error bars display S.E.M; bin size = 0.5 s). **Right**: average freezing
303 values during 10 s after CS onset and before NC response for CS^+ were higher than CS^- only at CS
304 onset (***, $P_{onset} = 0.0015$, paired t-test, n = 12 mice). **g.** Mean freezing values during fear
305 extinction, 24 CS^+ were presented across two separate extinction sessions (joined by dashed lines).
306 Mice acquired the CS^+-US association (1st CS^+ block vs. BL/CS^- ****, $P < 0.0001$, Friedman test,
307 n = 10 mice), followed by a rapid extinction (5th & 6th block of CS^+ vs BL/CS- ns, $P > 0.05$, one-
308 way RM ANOVA). **h.** After extinction, there was no difference in the NC response latency for
309 both CSs (ns, $P > 0.05$, paired t-test n = 10 mice). **i.** Average NC response latencies for the different
310 HP tests. *No tone* - mice submitted to the HP test without conditioning nor tone presentation. *Tone*
311 - mice submitted to the HP test paired with unconditioned tone presentation. *CS^-/CS^+* - mice were

312 submitted to the CFCA protocol. (No tone/Tone/CS^- vs. CS^+ **, $P < 0.0001$, Krustal-Wallis test).
313 For exact P values and test statistics on this and all subsequent figures, see Supplementary Table
314 1.

315 **Figure 2. SST^+ cells in vlPAG mediate the fear modulation of pain behavior. a.** Sst-IRES-Cre
316 mice were bilaterally injected with viruses that expressed ChR2 (right, upper), ArchT (right,
317 bottom), or GFP (control) in SST^+ vlPAG cells. **b**. Schematics of the stimulation protocol used for
318 photoactivation of the SST^+ vlPAG cells: blue light delivered at 2 Hz with 5 ms pulse duration
319 during CSs presentation until NC response. For photoinhibition experiments, green light was
320 delivered continuously. **c, e.** Average freezing values during retrieval for ChR2- (**c**) and ArchT-
321 infected mice (**e**) and their respective GFP controls. The opsin and respective control groups were
322 pooled together because no difference was found in the conditioning level (see Supplementary
323 Figure 4). Average freezing values during CS^+ were higher than CS^- or baseline (BL) periods (****,
324 $P < 0.001$, one-way RM ANOVA, (**c**) n = 16 mice and (**e**) n = 23 mice). **d.** Photoactivation of SST^+
325 vlPAG cells abolished the analgesic effect induced by fear (*, P = 0.0112, opsin x CS - two-way
326 RM ANOVA, n = 7 GFP, n = 9 ChR2). The NC response latency for the CS^+ was significantly
327 different between the ChR2 and GFP groups (*, P = 0.0344, Bonferroni post-hoc test). For the
328 ChR2 group, the NC response latency during CS^+ was equivalent to the CS^- (ns, P = 0.3876,
329 Bonferroni post-hoc test). On the contrary, NC response latency between the CSs differed in the
330 GFP group (***, P = 0.0003, Bonferroni post-hoc test). **f.** Photoinhibition of SST^+ vlPAG cells
331 increased the analgesic effect for the ArchT group when compared to the GFP (*, P = 0.0037, opsin
332 x CS - two-way RM ANOVA, n = 12 GFP, n = 11 ArchT). The NC response latency for the CS^-
333 and CS^+ was significantly different between the ArchT and GFP group (CS^-: ****, $P < 0.0001$,
334 Bonferroni post-hoc test; CS^+: *, P = 0.0265, Bonferroni post-hoc test). For the GFP group, the

335 latency of NC response was higher for the CS^+ trials when compared to the CS^- trials (***, P =
336 0.0003, Bonferroni post-hoc test), yet this was not the case for the ArchT group (ns, P > 0.999,
337 Bonferroni post-hoc test).

338 **Figure 3. Activation of SST^+ vlPAG cells reduced fear expression a.** Protocol for optogenetic
339 manipulation during fear retrieval. Days 1 and 2 were done as described previously for the CFCA
340 paradigm. During retrieval, there were 12 CS^+ presentations divided into three blocks. **b.** The
341 stimulation protocol used to photoactivate the SST^+ vlPAG cells. The optogenetic manipulation
342 was performed during the 2nd block of the CS^+ presentation (analogously to CFCA manipulations,
343 **Figure 2b**). **c.** Light inhibition of SST^+ vlPAG cells did not modulate freezing levels (ArchT ns, P
344 = 0.9396, opsin x CS two-way RM ANOVA, n = 6, GFP, n = 8). **d.** Photoactivation of the SST^+
345 vlPAG cells had no effect on the GFP group, but it transiently decreased the freezing levels for the
346 ChR2 group (***, P < 0.0001, opsin x CS two-way RM ANOVA, n = 9 GFP, n = 8 ChR2).

347 **Figure 4. Manipulation of SST^+ vlPAG cells alters spinal cord-related pain signals. a.**
348 Schematics of *in vivo* anesthetized experiments. Extracellular local field potential and single-unit
349 recordings in the spinal cord DH were performed during optogenetic stimulation of SST^+ vlPAG
350 cells with concomitant noxious electrical paw stimulation**. b.** Example of average nociceptive field
351 potentials in the lumbar SC before (OFF), during (ON), and after (OFF) photoactivation of SST^+
352 vlPAG cells (top). Photoactivation induces a significant increase in the nociceptive fields (bottom;
353 **, P = 0.0001, one-way RM ANOVA, n = 8 mice). **c.** Analogous to panel b, but for photoinhibition
354 of SST^+ vlPAG cells. Photoinhibition induces a significant decrease in the nociceptive fields
355 (bottom; *, P = 0.0275, one-way RM ANOVA, n = 5 mice). **d.** Example of WDR single-unit
356 activity before and during photoactivation of SST^+ vlPAG cells (**top**). Photoactivation of SST^+
357 vlPAG cells induces a significant and global increase in WDR response to both Aδ- and C-

358 mediated nociceptive fibers (**bottom**; **, $P_{A\delta\ fiber}$ = 0.0022, paired t-test, n = 11 cells; **, $P_{C\ fiber}$ <
359 0.0033, paired t-test, n = 11 cells). **e.** Analogous to panel d, but for photoinhibition of SST^+ vlPAG
360 cells. Photoinhibition induces a significant and specific inhibition of WDR response to Aδ- and C-
361 fibers (**bottom**; ***,** $P_{A\delta\ fiber}$ = 0.0241, ****, $P_{C\ fiber}$ < 0.0001, n = 14 cells**,** Wilcoxon matched-pairs
362 signed rank test). **f.** Example traces of single-unit recordings of WDR cells with subthreshold
363 electrical stimulation accompanied by photoactivation of SST^+ vlPAG cells (**top**). The
364 photoactivation of SST^+ vlPAG cells elicits WDR response to A- and C- mediated peripheral fibers
365 (**bottom**; *, $P_{A\delta\ fiber}$ = 0.0156, n = 10 cells; **, $P_{C\ fiber}$ = 0.0020, n = 10 cells, Wilcoxon matched-
366 pairs signed rank test).

367 **Figure 5. SST^+ vlPAG-RVM-DH pathway activation removes analgesia. a**. Schematics of
368 possible SST^+ vlPAG circuits mediating analgesia by long-range projections directly to the SC or,
369 alternatively, by projecting to the SC via the rostral ventromedial medulla (RVM). **b.** Sst-IRES-
370 Cre mice were injected with an anterograde AAV Cre-dependent GFP virus in the vlPAG (left).
371 Example of SST fibers labeling at the level of the RVM (middle)**.** Higher magnification (right)
372 reveals putative axonic buttons in the RVM (examples indicated by white arrows). **c.** Sst-IRES-
373 Cre mice were injected concomitantly with anterograde AAV Cre-dependent GFP virus in the
374 vlPAG and retrograde fluorogold in the lumbar DH of the SC. **d.** Fluorogold positive cells (red)
375 cross SST^+ vlPAG fibers in the RVM (green). Higher magnification (**right**) shows close contacts
376 between the putative SST^+ button and $fluorogold^+$ cells or fibers (white arrows). **e.** Sst-IRES-Cre
377 mice were injected in the vlPAG with AAV Cre-dependent ChR2 virus and an optic fiber placed
378 above the lumbar SC. Single-unit recordings of WDR cells while photoactivation of the SST^+
379 vlPAG SC fibers and electrically stimulating the paw in anesthetized mice (**left**). Photoactivation
380 of vlPAG projections to SC did not affect nociceptive transmission (**right**; ns, P = 0.3683, paired

381 t-test, n = 11 cells). **f.** Same experimental design as in panel e, except that the optic fiber was placed
382 above the RVM (left). Photoactivation of SST^+ vlPAG inputs to the RVM induces a significant
383 increase in WDR response to both Aδ- and C-mediated nociceptive fiber stimulation (**middle**; *,
384 $P_{A\delta\ fiber} = 0.0346$, Paired t-test, n = 10 cells; **, $P_{C\ fiber} = 0.0020$, Wilcoxon matched-pairs signed
385 rank test, n = 10 cells). Removal of analgesia by activation of SST^+ vlPAG-RVM induces a
386 significant increase in WDR response to C-fiber responses (right; **, P = 0.0078, Wilcoxon
387 matched-pairs signed rank test, n = 9 cells).

388

389 **Figure 6. SST^+ vlPAG-RVM-SC pathway activation abolishes analgesia induced by CFCA.**
390 **a.** Sst-IRES-Cre mice were bilaterally injected with an AAV expressing ChR2 or GFP in the
391 vlPAG, and optic fibers were implanted above the RVM (left). Representative example of SST^+
392 vlPAG terminals in the RVM (right). **b.** Photoactivation of SST^+ vlPAG-RVM pathway did not
393 modulate freezing levels (ns, P = 0.6443, opsin x CS two-way RM ANOVA; CS^+ 2nd block, GFP
394 vs. ChR2 ns, P > 0.9999, Bonferroni post-hoc test, n = 7 GFP, n = 6 ChR2). **c.** Average freezing
395 values during retrieval for pooled ChR2 and GFP-infected mice (groups were pooled together since
396 no difference was found in the conditioning level). Average freezing values during CS^+ were higher
397 than CS^- or baseline (BL) periods (****, P < 0.0001, one-way RM ANOVA, n = 14 mice). **d.**
398 Photoactivation of SST^+ vlPAG-RVM pathway abolished the analgesic effect modulated by fear
399 (**, P = 0.0063, opsin x CS - two-way RM ANOVA, n = 7 GFP, n = 7 ChR2). For the ChR2 group,
400 the NC response latency during CS^+ was equivalent to the CS^- (ns, P > 0.9999, Bonferroni post-
401 hoc test). On the contrary, the NC response latency between the CSs differed in the GFP group
402 (****, P < 0.0001, Bonferroni post-hoc test). **e**. Working model schematics for SST^+ control
403 analgesia induced during defensive states. Activation of SST^+ cells in the vlPAG is associated with

404 the inhibition of fear-induced freezing behavior. Selective activation of RVM projecting SST^+
405 vlPAG cells is associated with inhibition of analgesia induced during defensive states.
406

407 # Methods

408 **Subject details**

409 We used either male C57BL6/J mice (Janvier), heterozygous or homozygous Sst-IRES-Cre
410 mice (Jackson laboratory), or heterozygous VIP-IRES-Cre mice (Jackson Laboratory) age 8-14
411 weeks, that were individually housed under a 12 h light-dark cycle and provided with food and
412 water ad libitum. All procedures were performed in accordance with standard ethical guidelines
413 (European Communities Directive 86/60-EEC) and were approved by the committee on Animal
414 Health and Care of Institut National de la Santé et de la Recherche Médicale and the French
415 Ministry of Agriculture and Forestry (agreement #A3312001).
416

417 **Behavioral apparatus**

418 ***Cued fear-conditioned analgesia*** *task* was performed in three different contexts (**Figure 1a**).
419 Context A was used for *Habituation* and *Retrieval* and consisted of a plexiglass cylinder (25 x 24
420 cm diameter) with a grey, smooth plastic floor and house lights (16 lux). Context B was used for
421 *Fear conditioning* and consisted of a square plexiglass (25 x 40 cm) with a grid floor connected to
422 a shocker (Coulbourn Instruments) and brighter house lights (40 lux). A total of 5 scrambled
423 footshocks of 1 s duration and intensity of 0.8 mA were delivered via the grid floor and served as
424 the unconditioned stimulus (US). Contexts A and B were cleaned, respectively, with 70% ethanol
425 or 1 % acetic acid between different mice. Both contexts contained infrared beam detection that

426 automatically scored freezing periods, determined by no change in infrared beam crossing for at
427 least 2 s.

428 Context C was used for the *FC Hot Plate (HP) test*. A steady increase in temperature was
429 controlled by the Incremental Hot/Cold Plate Analgesia Meter (IITC) device. To restrain the mice's
430 movement, the HP apparatus had a testing surface (plate) enclosed in a square plexiglass surface
431 (20.3 x 10 x 20.5 cm) and house lights (100 lux). The mice's temperature and surroundings were
432 recorded using an infrared digital thermographic camera (Testo 885) placed ~ 50 cm above the
433 testing surface. The thermal camera had a spatial resolution of 320 × 240 pixels, a sampling rate of
434 25 Hz, and thermal sensitivity of 0.03 °C at 30 °C. The testing surface of context C was cleaned
435 with water between different mice. All three contexts were enclosed in an acoustic foam isolated
436 box with speakers mounted on the top of each compartment. The auditory conditioned stimulus
437 (CS) consists of either 7.5 kHz or white-noise 50 ms pips at 1 Hz, repeated 27 times, with 2 ms rise
438 and fall, and a sound pressure level of 80 dB.

439 ***Open field*** *task* was performed in a square plexiglass arena (36 x 36 x 25cm). A LED mounted
440 on the top-right side of the arena signaled the start and end of different epochs for offline analyses.
441 A video camera recorded from above the arena at 30 fps for offline video-tracking purposes.

442 ***Real-Time Place Preference (RTPP)*** *task* was performed in a shuttlebox consisting of a
443 plexiglass box (40 x 10 x 30 cm) with a floor grid, where a small plastic hurdle (1 cm height)
444 divided the arena into two equal compartments, while infrared beam detection automatically
445 monitored the mice shuttling between compartments (Imetronic). A video camera recorded from
446 above the arena at 30 fps for offline video-tracking purposes.

447 For both the open field and RTPP tasks, a free user video-tracking software (idTracker: Tracking
448 individuals in a group by automatic identification of unmarked animals) together with in-house
449 codes in Matlab (The MathWorks, Inc., Natick, MA, USA) was used to analyze each condition.

450 **Behavioral paradigm**

451 ***Cued fear-conditioned analgesia (CFCA).*** C57BL6/J mice (n = 12) were habituated to the
452 context and tones (day 1). Four white-noise (CS^-) and four 7.5 kHz (CS^+) tones were presented
453 sequentially and without US reinforcement. In Fear conditioning (day 2), five CS^- and five CS^+
454 were presented in an intermingled fashion. The CS^+ presentations were paired with a mild
455 footshock (US) at tone offset, whereas the CS^- was never reinforced. The Fear retrieval session
456 (Day 3) was done 24h after conditioning and in the same context as the habituation session. As in
457 habituation, four CS^- and four CS^+ were presented sequentially and without US reinforcement
458 (**Figure 1a**).

459 Since the focus of this study was the emotional modulation of pain sensitivity, it was compulsory
460 to evaluate the associative fear levels before measuring their impact on pain sensitivity. Two
461 indices were computed: the discrimination index (DI), to assess the discrimination between CS^-
462 and CS^+, and the conditioning index (CI), which indicated the level of freezing to the tone
463 predicting the US. These indexes were calculated as follows: $\mathrm{DI} = \frac{(Freezing\ to\ CS+)-(Freezing\ to\ CS-)}{(Freezing\ to\ CS+)+(Freezing\ to\ CS-)}$
464 and CI = DI × (Freezing to CS^+). Based on preliminary data, mice were only submitted to the FC
465 HP test if DI ≥ 0.4 & CI ≥ 0.3. Mice that did not fit the criteria were conditioned a second time.
466 There was a minimum interval of 2 h between the retrieval and the FC HP test.

467 The FC HP test consisted of two trials, one in which the CS^+ was presented and another in which
468 the CS^- was presented. The two trials were counterbalanced within the group. The testing surface
469 was set at 30 ºC**.** After a 60 s acclimatization period, its temperature gradually increased at 6 ºC per
470 minute (HP start). Tone presentation (CS^+ or CS^-) started 130 s after the HP start. Temperature
471 increase and tone presentation terminated concomitantly with the display of a nociception response.
472 Valid nociception readout responses included jumping or licking the hindpaw. The effect of the

473 negative emotional modulation on pain sensitivity was assessed by comparing the latency (or
474 temperature) of the NC response between the two HP trials. There was a minimum of 30 min
475 interval between the two trials for each mouse, during which mice returned to their home cage.

476 Freezing during the HP test was assessed by automatically analyzing thermographic camera
477 videos using custom scripts (available at: github.com/djercog/TestoFreez). Briefly, individual
478 video frames were binarized to define a mask for the mouse within each frame. Consecutive
479 binarized frames were then subtracted, and the number of non-zero pixels in the resultant image
480 determined if the mouse was considered immobile when below a certain threshold (defined to
481 approximate manual freezing estimation on random videos). Immobilization episodes of at least
482 0.5 s were considered as freezing periods. In contrast, non-immobilization episodes shorter than
483 0.1 s were merged together with the neighbouring detected freezing episodes.

484 ***Extinction training.*** On days 3 and 4, mice (n =10) were submitted to an extinction training
485 protocol established by Courtin et al. 2014[41]. Briefly, there were 4 CS^- and 12 CS^+, presented in a
486 non-reinforced manner (**Figure 1g**). Mice were considered to have successfully extinguished the
487 fear expression if the level of freezing in the last 4 CS^+ was not statistically different from the CS^-
488 . After fear extinction, mice were submitted to the FC HP test, using the same parameters as in the
489 CFCA paradigm.

490 ***Stability training***. The first three days consisted of the classical CFCA paradigm. On day 4,
491 mice (n = 10) repeated the protocol applied on day 3 (**Supplementary Figure 2e-i)**. All mice that
492 met the fear conditioning criteria (DI ≥ 0.4 & CI ≥ 0.3) on day 3 were kept for the following day,
493 independent of their level of Conditioning on day 4.

494 ***Vasoconstriction assay.*** To determine whether vasoconstriction was a confounding factor in the
495 FC HP test outcomes, we used a modified version of the CFCA paradigm (**Figure 1f)**. During the
496 HP test (n = 13), the temperature was not gradually increased but maintained at 30 ºC while CSs

497 were presented. The tones (CS^+ or CS^-) were presented for 120 s, and mice were kept for an
498 additional 50 s before the HP trial terminated. Offline, with the infrared videos, mice's back and
499 tail were measured at 30 s intervals. For each measurement point, the temperatures of three spots
500 on the back and tail were averaged to obtain the body temperature for each body part at that time
501 point and mouse.

502 ***Basal nociception assay (No tone).*** Naïve mice (n = 10) were submitted to the HP test (**Figure**
503 **1i and Supplementary Figure 2a-d)**. Each mouse underwent two identical trials. The HP test was
504 similar to the one described in the CFCA paradigm, except no tones were presented. There was a
505 minimum of 30 min interval between the two trials, during which mice returned to a restful state
506 in their home cage. Since the two trials were not significantly different, for simplicity, in panel i of
507 Figure 1, the two trials were pooled together.

508 ***Tone-specific nociception assay.*** Naïve mice (n = 12) were submitted to the HP test without
509 auditory fear conditioning (**Figure 1i and Supplementary Figure 2a-d)**. Each animal underwent
510 two trials, one trial with a 7.5 kHz tone presentation and another with a WN tone presentation. The
511 tone presentation was counterbalanced. The HP test parameters were similar to those described for
512 the CFCA, except that both tones were unconditioned. Since the two trials were not significantly
513 different, for simplicity, in panel i of Figure 1, the two trials were pooled together.

514 ***Open Field assay.*** This test was used to determine the effect of optogenetic stimulation on
515 locomotion. Therefore, only mice from optogenetic experiments were submitted to this assay. Mice
516 could freely move during the entire test. The locomotion assay had a total duration of 9 min and
517 was divided into 3 min epochs. The first and third epochs were OFF periods in which no optical
518 stimulation occurred. During the second epoch, mice received photostimulation (ON period). The
519 optogenetic stimulation effect was analyzed by comparing the overall distance traveled between
520 the OFF and ON epochs (**Supplementary Figure 5c, d)**. Mice injected with GFP were used to test

521 the effect of heat and light on the stimulation itself. Mouse tracking data were extracted from video
522 recordings using idTracker[42] and imported into Matlab for further analysis with custom scripts to
523 calculate the total distance traveled during stimulation.

524 ***Real-time Place Preference assay.*** Only mice from optogenetic experiments were submitted to
525 this assay. During the entire duration of the assay, mice could freely shuttle between the two
526 compartments. Under closed-loop stimulation, mice received photo-stimulation upon entry into
527 one of the two compartments. The stimulated compartment was counterbalanced within the group.
528 The optical stimulation effect was assessed by comparing the time spent in the stimulated
529 compartment between the ChR2 and GFP groups (**Supplementary Figure 5e, f**). Permanence time
530 in the stimulated compartment was automatically assessed by the apparatus software (Imetronic).

531 **Virus injections and optogenetics**

532 For optogenetic manipulation of SST^+ cells in the vlPAG, 0.15-0.2 µL of either ChR2 (AAV5-
533 EF1a-DIO-hChR2(H134R)-EYFP, titer: $3.2x10^{12}$ - Vector Core, University of North Carolina),
534 ArchT (AAV9-CAG-FLEX-ArchT-GFP, titer: $4.7x10^{12}$ - Vector Core, University of North
535 Carolina) or GFP (AAV5-FLEX-GFP, titer: $4.5x10^{12}$ - Vector Core, University of North Carolina)
536 were bilaterally injected into the vlPAG of 8/9 weeks old Sst-IRES-Cre mice from glass pipettes
537 (tip diameter 20-30 µm) at the following coordinates relative to bregma: - 4.4 mm AP; ± 1.5 mm
538 ML; -2.45 mm DV from dura, with a 20 degrees angle. Injection coordinates for manipulating VIP^+
539 vlPAG cells were as follows: - 4.4 mm AP; ± 1.35 mm ML; -2.5 mm DV from dura, with a 20
540 degrees angle.

541 At two weeks after the injections, mice were bilaterally implanted with custom-built optic fibers
542 (diameter: 200 µm; numerical aperture: 0.39; Thorlabs) above the vlPAG at the following
543 coordinates relative to bregma: i) Sst-IRES-Cre mice: - 4.4 mm AP; ± 1.0 mm ML; -1.8 mm DV

544 from dura, with a 10 degrees angle; ii) VIP-IRES-Cre mice: - 4.4 mm AP; ± 0.8 mm ML; -2.0 mm
545 DV from dura, with a 10 degrees angle. For RVM manipulations, mice were implanted at the
546 following coordinates relative to bregma: -5.8 mm AP; 0.0 mm ML; -5.2 DV from the dura. All
547 implants were secured using three stainless steel screws and Super-Bond cement (Sun Medical).
548 During surgery, long- and short-lasting analgesic agents were injected (Metacam, Boehringer;
549 Lurocaïne, Vetoquinol). After surgery, mice were allowed to recover for at least five days.
550 Afterward, mice were handled daily to familiarize themselves with being restrained for the optic
551 fibers connection. Behavioral experiments were performed at least four weeks after viral injections.
552 Only mice with correct placement of optic fibers and virus expression were included in the
553 analyses.

554 For optogenetic excitation, light stimulation consisted of blue light (473 nm, ~8-10 mW at fiber
555 tip) delivered with 2 Hz frequency and 5 ms pulse duration. In contrast, light stimulation consisted
556 of green light (532 nm, ~8-10 mW at fiber tip) delivered continuously for optogenetic inhibition.
557 For optogenetic manipulations during the CFCA paradigm of either SST^+ or VIP^+ vlPAG cells, the
558 light was delivered during the FC HP test and paired with the tone presentation.

559 Two sets of experiments were performed sequentially for stimulation during the fear
560 conditioning. First, the footshock US was replaced by optical stimulation. Then, the US became
561 the optical stimulation combined with the footshock (**Supplementary Figure 6**). For both
562 conditions, optogenetic stimulation began 5 s before and lasted until 5 s after CS^+ offset. The same
563 mice were used for both experiments. For the manipulations during the fear retrieval, there were
564 12 CS^+ presentations divided into blocks of 4 CS^+. The optogenetic stimulation was paired with
565 the second block of CS^+.

566

567 **Single-molecule *in situ* hybridization**

568 Expression of *Sst*, *Slc31a1*, *Slc17a6,* and *Cre* transcripts was detected in C57/BL6J mice using
569 single-molecule fluorescent *in situ* hybridization (smFISH) as previously described (Castell et al.,
570 2024 PMID: 37858736). Briefly, coronal PAG sections (16 µm) were collected directly onto
571 Superfrost Plus slides. Probes for *Sst* (ACDBio; Cat#404631), *Slc32a1* (ACDBio; Cat#319191-
572 C2), *Slc17a6* (ACDBio; Cat#319171-C2), and *Cre* (ACDBio; Cat#312281-C2) were used with the
573 RNAscope Fluorescent Multiplex Kit (ACDBio; Cat# 323110). Fluorescence was captured using
574 sequential laser scanning confocal microscopy (Leica SP8), and quantification was performed in
575 ImageJ.

576 **Anatomical tracing**

577 ***Fluorogold injection.*** An incision between one to two cm was made slightly caudal to the peak
578 of the dorsal hump to expose the lumbar spinal region. The vertebra of interest was identified.
579 Then, a small incision was made between the tendons and the vertebral column on either side. The
580 vertebra was then secured using spinal adaptor clamps, and all tissue was removed from the surface
581 of the bone. Pulled borosilicate glass capillaries (Ringcaps, disposable capillary pipettes with ring
582 mark, DURAN, Hirschmann Laborgeräte, Germany) were inserted between 2 vertebrae and
583 allowed to microinject 0.5 µL of fluorogold 2% in the dorsal horn of the spinal cord on both sides.

584 ***In vivo* electrophysiology**

585 Mice were anesthetized with isoflurane 4% for induction, then 1.5% maintenance. The
586 experiment was started as soon as there was no longer any reflex. The colorectal temperature was
587 kept at 37 °C with a heating blanket. Two metal clamps were used to stabilize the animal's spine
588 in a stereotactic frame (M2E, France) during electrophysiological recordings. Then, a laminectomy
589 was performed at T13-L1 to expose the lumbar part of the spinal cord. The dura mater was carefully
590 removed. Custom-made optical fibers were placed 1mm above the dorsal spinal cord for

591 optogenetic manipulations. C-fiber-evoked field potentials were recorded in the deep lamina of the
592 DH (at a depth range of 250 and 500 µm) with borosilicate glass capillaries (2 MΩ, filled with
593 NaCl 684 mM; Harvard Apparatus, Cambridge, MA, USA). Field potentials were recorded with
594 an ISODAM-amplifier (low filter: 0.1Hz to high filter: 0.1 kHz; World Precision Instruments,
595 USA) in response to electrical stimulation of the ipsilateral paw. Single unit recordings of WDR
596 DH cells were made with the same borosilicate glass capillaries mentioned above and placed in the
597 dorsal part of the spinal cord. The criterion for selecting a cell was the presence of an A-fiber-
598 evoked response (0-80 ms) followed by a C-fiber-evoked response (80-150 ms) to electrical
599 stimulation of the ipsilateral sciatic nerve.

600 The paw of the mice was stimulated by trains (every 30 s) of electrical stimulation at two times
601 the threshold for C-fibers, which were performed before, during, and after optogenetic stimulations
602 with an optic fiber placed above the recording site. Subthreshold stimulations were performed
603 below the threshold for C-fiber and A-fiber, respectively.

604 **Histology analyses**

605 Mice were administered a lethal dose of Exagon and underwent transcardial perfusions via the
606 left ventricle with 4% w/v paraformaldehyde (PFA) in 0.1 M PB. Following dissection, brains were
607 post-fixed for 24 h at 4°C in 4% PFA. Brain sections of 80 µm-thick were cut on a vibratome,
608 mounted on gelatin-coated microscope slides, and dried. To verify correct viral injections and optic
609 fiber location, serial 80 µm-thick slices containing the regions of interest were mounted in
610 VectaShield (Vector Laboratories) and imaged using an epifluorescence system (Leica DM 5000)
611 fitted with a 10-x dry objective. The location and the extent of the injections/infections were
612 visually controlled. Only infections targeting the vlPAG and optic fibers terminating, depending
613 on the experiment, above the vlPAG or RVM were included in the analyses.

614 **Statistics**

615 All statistical details are contained in Supplementary Table 1. Box-whisker plots indicate
616 median, interquartile range, and 5th - 95th percentiles of the distribution. All statistics are indicated
617 where used. Statistical analyses were performed with Prism software (GraphPad). We tested the
618 normality of all data with the Kolmogorov–Smirnov normality test in Prism software (GraphPad),
619 and used nonparametric statistical tests for nonnormally distributed datasets, as indicated where
620 used. No statistical methods were used to predetermine sample sizes, but sample sizes were based
621 on previous studies in our laboratory. Blinding for the opsin was done for optogenetics
622 experiments. Animals used for the CFCA paradigm that did not satisfy the DI and CI criteria after
623 two conditioning sessions were discarded from the study. Mice with an incorrect injection of the
624 opsins or misplaced location of the optic fibers were discarded. For *in vivo* electrophysiology, field
625 potentials were measured as the area above the curve in the C-fiber range (80-300 ms). Absolute
626 values were used to compare values in each condition (OFF vs. ON optogenetic manipulation). In
627 single-unit recordings, the number of A- and C-fiber induced spikes in WDR cells was measured
628 after each electrical stimulation, during, and after optogenetic manipulation. An average of the four
629 stimuli for each WDR recorded was used for statistical analysis. Outliers were removed using the
630 Tukey method.

631 No other mice were excluded. Significance levels are indicated as follows: *$p<0.05$, **$p<0.01$,
632 ***$p<0.001$, **** $p<0.0001$.

633 **Data and script availability**

634 Data supporting the findings of this study, including analysis codes, are available from the
635 corresponding author upon request.

636

637 ## References

638 1. Bolles, R. C. & Fanselow, M. S. A perceptual-defensive-recuperative model of fear and pain.
639 *Behav. Brain Sci.* **3**, 291–301 (1980).
640 2. Rhudy, J. L. & Meagher, M. W. Fear and anxiety: divergent effects on human pain
641 thresholds. *Pain* **84**, 65–75 (2000).
642 3. Flor, H. & Grösser, S. M. Conditioned stress-induced analgesia in humans. *Eur. J. Pain* **3**,
643 317–324 (1999).
644 4. Beckham, J. C. *et al.* Chronic posttraumatic stress disorder and chronic pain in Vietnam
645 combat veterans. *J. Psychosom. Res.* **43**, 379–389 (1997).
646 5. International Association for the Study of Pain. IASP Terminology. Iasp (2017).
647 6. Butler, R. K. & Finn, D. P. Stress-induced analgesia. *Prog. Neurobiol.* **88**, 184–202 (2009).
648 7. Rea, K., Roche, M. & Finn, D. P. Modulation of Conditioned Fear, Fear-Conditioned
649 Analgesia, and Brain Regional C-Fos Expression Following Administration of Muscimol into
650 the Rat Basolateral Amygdala. *J. Pain* **12**, 712–721 (2011).
651 8. Floyd, N. S., Price, J. L., Ferry, A. T., Keay, K. A. & Bandler, R. Orbitomedial prefrontal
652 cortical projections to distinct longitudinal columns of the periaqueductal gray in the rat. *J.*
653 *Comp. Neurol.* **422**, 556–578 (2000).
654 9. LeDoux, J., Iwata, J., Cicchetti, P. & Reis, D. Different projections of the central amygdaloid
655 nucleus mediate autonomic and behavioral correlates of conditioned fear. *J. Neurosci.* **8**,
656 2517–2529 (1988).
657 10. Vertes, R. P. Differential projections of the infralimbic and prelimbic cortex in the rat.
658 *Synapse* **51**, 32–58 (2004).

659 11. Carrive, P. & Morgan, M. M. Periaqueductal Gray - Chapter 10. The Human Nervous 631
660 System (Elsevier, 2012). doi:10.1016/B978-0-12-374236-0.10010-0.
661 12. Basbaum, A. I. & Fields, H. L. Endogenous Pain Control Systems: Brainstem Spinal
662 Pathways and Endorphin Circuitry. *Annu. Rev. Neurosci.* **7**, 309–338 (1984).
663 13. Millan, M. J. Descending control of pain. *Prog. Neurobiol.* **66**, 355–474 (2002).
664 14. Fields, H. L., Heinricher, M. M. & Mason, P. Neurotransmitters in Nociceptive Modulatory
665 Circuits. *Annu. Rev. Neurosci.* **14**, 219–245 (1991).
666 15. Samineni, V. K. *et al.* Divergent Modulation of Nociception by Glutamatergic and
667 GABAergic Neuronal Subpopulations in the Periaqueductal Gray. *eneuro* **4**, ENEURO.0129-
668 16.2017 (2017).
669 16. V., C., C., M. & M., B. Role of benzodiazepine and serotonergic mechanisms in conditioned
670 freezing and antinociception using electrical stimulation of the dorsal periaqueductal gray as
671 unconditioned stimulus in rats. *Psychopharmacology (Berl.)* **165**, 77–85 (2002).
672 17. Helmstetter, F. J. & Landeira-Fernandez, J. Conditional hypoalgesia is attenuated by
673 Naltrexone applied to the periaqueductal gray. *Brain Res.* **537**, 88–92 (1990).
674 18. Bellgowan, P. S. F. & Helmstetter, F. J. The role of mu and kappa opioid receptors within the
675 periaqueductal gray in the expression of conditional hypoalgesia. *Brain Res.* **791**, 83–89
676 (1998).
677 19. Jacquet, Y. F. The NMDA receptor: central role in pain inhibition in rat periaqueductal gray.
678 *Eur. J. Pharmacol.* **154**, 271–276 (1988).
679 20. Moreau, J. L. & Fields, H. L. Evidence for GABA involvement in midbrain control of
680 medullary neurons that modulate nociceptive transmission. *Brain Res.* **397**, 37–46 (1986).

681 21. Osborne, P. B., Vaughan, C. W., Wilson, H. I. & Christie, M. J. Opioid inhibition of rat
682 periaqueductal grey neurones with identified projections to rostral ventromedial medulla in
683 vitro. *J. Physiol.* **490**, 383–389 (1996).
684 22. Harris, J. A. Descending antinociceptive mechanisms in the brainstem: Their role in the
685 animal's defensive system. *J. Physiol.-Paris* **90**, 15–25 (1996).
686 23. Tovote, P. *et al.* Midbrain circuits for defensive behaviour. *Nature* **534**, 206–212 (2016).
687 24. Lau, B. K. & Vaughan, C. W. Descending modulation of pain: the GABA disinhibition
688 hypothesis of analgesia. *Curr. Opin. Neurobiol.* **29**, 159–164 (2014).
689 25. Fields, H. State-dependent opioid control of pain. *Nat. Rev. Neurosci.* **5**, 565–575 (2004).
690 26. Ossipov, M. H., Dussor, G. O. & Porreca, F. Central modulation of pain. *J. Clin. Invest.* **120**,
691 3779–3787 (2010).
692 27. Vianna, D. M. L. & Carrive, P. Changes in cutaneous and body temperature during and after
693 conditioned fear to context in the rat. *Eur. J. Neurosci.* **21**, 2505–2512 (2005).
694 28. Smith, G. S. T. *et al.* Distribution of messenger RNAs encoding enkephalin, substance P,
695 somatostatin, galanin, vasoactive intestinal polypeptide, neuropeptide Y, and calcitonin gene-
696 related peptide in the midbrain periaqueductal grey in the rat. *J. Comp. Neurol.* **350**, 23–40
697 (1994).
698 29. Viollet, C. *et al.* Somatostatin-IRES-Cre Mice: Between Knockout and Wild-Type? *Front.*
699 *Endocrinol.* **8**, 131 (2017).
700 30. Gasser, H. S. The classification of nerve fibers. Ohio J. Sci. (1941).
701 31. Mogil, J. S. Sex differences in pain and pain inhibition: multiple explanations of a
702 controversial phenomenon. *Nat. Rev. Neurosci.* **13**, 859–866 (2012).
703 32. Aby, F. *et al.* Switch of serotonergic descending inhibition into facilitation by a spinal
704 chloride imbalance in neuropathic pain. *Sci. Adv.* **8**, eabo0689 (2022).

705 33. Grivet, Z. *et al.* Brainstem serotonin amplifies nociceptive transmission in a mouse model of
706 Parkinson's disease. *Npj Park. Dis.* **11**, 11 (2025).
707 34. Tovote, P., Fadok, J. P. & Lüthi, A. Neuronal circuits for fear and anxiety. *Nat. Rev.*
708 *Neurosci.* **16**, 317–331 (2015).
709 35. Yin, W. *et al.* A Central Amygdala–Ventrolateral Periaqueductal Gray Matter Pathway for
710 Pain in a Mouse Model of Depression-like Behavior. *Anesthesiology* **132**, 1175–1196 (2020).
711 36. Zhang, Y. *et al.* Somatostatin Neurons from Periaqueductal Gray to Medulla Facilitate
712 Neuropathic Pain in Male Mice. *J. Pain* **24**, 1020–1029 (2023).
713 37. Morgan, M. M., Whittier, K. L., Hegarty, D. M. & Aicher, S. A. Periaqueductal gray neurons
714 project to spinally projecting GABAergic neurons in the rostral ventromedial medulla. *Pain*
715 **140**, 376–386 (2008).
716 38. Butler, R. K. *et al.* Molecular and electrophysiological changes in the prefrontal cortex–
717 amygdala–dorsal periaqueductal grey pathway during persistent pain state and fear-
718 conditioned analgesia. *Physiol. Behav.* **104**, 1075–1081 (2011).
719 39. Tovote, P., Esposito, M. S., Botta, P., Chaudun, F. & Jonathan, P. Midbrain circuits for
720 defensive behaviour. *Nat. Press* https://doi.org/10.1038/nature17996 (2016)
721 doi:10.1038/nature17996.
722 40. McWilliams, L. A., Cox, B. J. & Enns, M. W. Mood and anxiety disorders associated with
723 chronic pain: an examination in a nationally representative sample. *Pain* **106**, 127–133
724 (2003).
725 41. Courtin, J. *et al.* Prefrontal parvalbumin interneurons shape neuronal activity to drive fear
726 expression. *Nature* **505**, 92–6 (2014).

42. Pérez-Escudero, A., Vicente-Page, J., Hinz, R. C., Arganda, S. & De Polavieja, G. G. idTracker: tracking individuals in a group by automatic identification of unmarked animals. *Nat. Methods* **11**, 743–748 (2014).

Acknowledgments

We thank Joshua Johansen, David Finn, and Nadine Gogolla for critical and stimulating discussions; K. Deisseroth and E. Boyden for generously sharing material, S. Laumond, J. Tessaire, and the technical staff of the housing and experimental animal facility of the Neurocentre Magendie. We thank Claire Francioni for her technical support. Microscopy was performed in the Bordeaux Imaging Center of the CNRS-INSERM and Bordeaux University, member of France BioImaging. This work was supported by grants from the French National Research Agency (ANR-FEARLESSPAIN, ANR-10-EQPX-08 OPTOPATH), the Fondation pour la Recherche Médicale (FRM-PhD grant to NW 2020-2021) and the French Society for the Study and Treatment of Pain (SFETD – grant to NW 2022).

Author Contributions

N.W performed behavioral experiments and optogenetic experiments on freely moving animals. F.A, J.V, performed electrophysiological and optogenetic experiments on anesthetized animals. E.V, L.C, N.W, F.A, Z.G, C.R, R.B, and D.G performed histology. N.W, M.L, S.V. P.F, and C.H. designed the experiments. N.W, F.A, D.J, and E.V analyzed the data, N.W, D.J. and C.H wrote the paper.

749 ## Supplementary Figures

750 **Supplementary Figure 1. Cued fear-conditioned analgesia behavior. a.** During habituation, the
751 freezing levels for the context (BL) and the two tones were low but significantly different (****, P
752 = 0.0003, Friedman test, n = 12 mice). **b.** Mean temperature at which the NC response was observed
753 in the HP test. The temperature of NC response was higher during CS^+ trials when compared to the
754 CS^- trials (***, P = 0.0005, Wilcoxon matched-pairs signed rank test, n = 12 mice)**. c.** Schematic
755 representation of how the back and tail temperature of the mice was measured. Every 30-sec three-
756 point temperature was taken for each of the two body parts. The temperature of the mice back and
757 tail were measured by the infrared digital thermographic camera and analyzed offline (see
758 Methods). The average temperature of the mice back (**d**) and tail (**e**) while the CS^+ or the CS^- were
759 presented. There were no differences in body temperature for the different CSs trials (ns, P > 0.05,
760 mixed-effects model, n = 13 mice). Vertical dashed lines correspond to the average time of NC
761 response for the CS^+ (red) and CS^- (blue) during the standard CFCA protocol.

762 **Supplementary Figure 1. CFCA depends on associative processes. a. Top**, protocol for the *No*
763 *Tone*: naïve mice were submitted to two HP trials without conditioning nor tone presentation.
764 **Bottom**, protocol for the *Tone*: naïve mice were submitted to two HP trials paired with an
765 unconditioned tone presentation. **b, c.** Mean latency and temperature of NC response for the two
766 tests mentioned above and the CFCA. The transient cued-fear induced analgesia (CS^+) compared
767 to the basal nociception, the tone, and the CS^- trials (***, P = 0.0001, Krustal-Wallis test). Trials
768 between the same type of test (*No tone* or *Tone*) were not significantly different (ns, P > 0.05,
769 Bonferroni post-hoc test, see statistical table for all comparisons) **d.** After fear extinction, there was
770 no difference in the mean temperature response between the two CSs (ns, P = 0.3276 paired t-test,
771 n = 10 mice). **e.** Protocol for stability training (see methods). Mice were submitted to two rounds

772 of the CFCA paradigm. During retrieval (**f, g**), average freezing values during CS^+ was higher than
773 CS^- or baseline (BL) periods (****, $P < 0.0001$, one-way RM ANOVA, n = 10 mice). **h, i.** Mean
774 latency and temperature of NC response during CS^- and CS^+ trials for FC HP test 1 (**h**) and test 2
775 (**i**). CS^+ presentation increased the latency and temperature of NC response in FC HP test 1 and test
776 2 (*, **, and ***, $P < 0.05$, paired t-test; for details, see supplementary table 1).

777 **Supplementary Figure 3. Two distinct neuronal populations in SST- Cre mice within the**
778 **PAG. a.** Representative picture of single-molecular fluorescent in situ hybridization for Sst
779 mRNAs in the PAG. Scale bar, 400 µm. **b, c.** Single-molecular fluorescent in situ hybridization for
780 Sst (green) and Cre (red) mRNAs in the vlPAG (left). Histograms showing the co-expression of
781 Sst/Cre as percentage of Sst-expressing cells (green) and as percentage of Cre-expressing cells
782 (red) in the dlPAG and vlPAG (right). Scale bar, 20 µm. In the dlPAG, 94% of RNA SST-
783 expressing-cells (101 out of 107 cells) expressed Cre RNA, and 84 % of RNA Cre-expressing cells
784 expressed somatostatin RNA (101 out of 20 cells). In the vlPAG, the values are 88% (74 out of 84
785 cells) and 99% (74 out of 75 cells) for Cre and SST, respectively. **d.** Single-molecular fluorescent
786 in situ hybridization for Sst (red) and Slc32a1 (green) within the dlPAG (upper panel) and vlPAG
787 (bottom panel). Scale bar, 20 µm. **e.** Quantification of colocalization within the dlPAG (upper
788 panel) and vlPAG (bottom panel) of Sst^+ and $Slc32a1^+$. In the dlPAG, approximately 19% of
789 $Slc32a1^+$ cells (17 out of 80 cells) are Sst^+, and 17% (17 out of 88 cells) of Sst^+ cells are $Slc32a1^+$.
790 On the contrary, in the vlPAG, approximately 95% of $Slc32a1^+$ cells (183 out of 186 cells) are Sst^+,
791 and 61% of Sst^+ cells (183 out of 254 cells) are $Slc32a1^+$. **f.** Single-molecular fluorescent in situ
792 hybridization for Sst (red) and Slc17a6 (green) within the dlPAG (upper panel) and vlPAG (bottom
793 panel). Scale bar, 20 µm. **g.** Quantification of colocalization within the dlPAG (upper panel) and
794 vlPAG (bottom panel) of Sst^+ and $Slc17a6^+$. In the dlPAG, approximately 91% of $Slc17a6^+$ cells

795 (54 out of 61 cells) are Sst^+, and 38% of Sst^+ cells (54 out of 172 cells) are $Slc17a6^+$. On the
796 contrary, in the vlPAG, approximately 34% of $Slc17a6^+$ cells (43 out of 176 cells) are Sst^+ and 33%
797 of Sst^+ cells (43 out of 115 cells) are $Slc17a6^+$. White arrows indicate colocalization.

798 **Supplementary Figure 4. Comparable fear levels prior to the FC HP test**. After retrieval, fear
799 conditioning levels between the opsins and their respective GFP groups were tested to ensure
800 equivalent fear levels. The discrimination index (see methods) between the GFP and ChR2 (**a**, ns,
801 P = 0.6052 unpaired t-test, n = 16 mice) or ArchT (**b,** ns, P = 0.4575, unpaired t-test, n = 23 mice)
802 were not significantly different. All the mice discriminated equally between CSs. The conditioning
803 index (see methods) between the GFP and ChR2 (**c,** ns, P = 0.2333, unpaired t-test n = 16 mice) or
804 ArchT (**d,** ns, P = 0.1320, unpaired t-test, n = 23 mice) were also not significantly different. All
805 mice displayed a similar high freezing level to the CS^+.

806 **Supplementary Figure 5. Optogenetic manipulation of SST^+ vlPAG cells does not affect**
807 **locomotion or produce aversion. a.** Photoactivation of SST^+ vlPAG cells abolished the analgesic
808 effect induced during defensive states (**, P = 0.0035, opsin x CS - two-way RM ANOVA, n = 7
809 GFP, n = 9 ChR2). The mean temperature of NC response for the CS^+ was significantly different
810 between the ChR2 and GFP groups (*, P = 0.0322, Bonferroni post-hoc test). For the ChR2 group,
811 the mean temperature of NC response during CS^+ was equivalent to the CS^- (ns, P = 0.1783,
812 Bonferroni post-hoc test). On the contrary, the mean temperature of NC response between the CSs
813 differed for the GFP group (****, P < 0.0001, Bonferroni post-hoc test). **b.** Photoinhibition of SST^+
814 vlPAG cells increased the analgesic effect for the ArchT group when compared to the GFP (**, P
815 = 0.0035, opsin x CS - two-way RM ANOVA, n = 12 GFP, n = 11 ArchT). The mean temperature
816 of NC response for the CS^- was significantly different between the ArchT and GFP groups (****,
817 P < 0.0001, Bonferroni post-hoc test). For the GFP group, the mean temperature of NC response

818 was higher for the CS^+ trials when compared to the CS^- trials (***, P = 0.0003, Bonferroni post-
819 hoc test), yet this was not the case for the ArchT group (ns, P > 0.999, Bonferroni post-hoc test).
820 **c.** The photoactivation of SST^+ vlPAG cells was performed during the ON epoch (blue shaded
821 area), and the average distance traveled during the ON epoch was not different from the OFF
822 epochs when comparing the two opsins (ns, P = 0.5121, opsin x light - two-way RM ANOVA, n =
823 7 GFP, n = 9 ChR2). **d.** The photoinhibition of SST^+ vlPAG cells was performed during the ON
824 epoch (yellow shaded area), and the average distance traveled during the ON epoch was not
825 different from the OFF epochs when comparing the two opsins (ns, P =0.4047, opsin x light - two-
826 way RM ANOVA, n = 12 GFP, n = 11 ArchT). **e.** Real-time place-preference location plot from a
827 representative animal while submitted to optogenetic activation of SST^+ vlPAG cells in the left
828 compartment throughout the 15-min session. **f**. There was no difference between ChR2- expressing
829 mice and the control group in the time spent in the stimulated and non-stimulated compartments
830 (ns, P = 0.1812, Mann-Whitney test).

831 **Supplementary Figure 6. SST^+ vlPAG cells photoactivation during conditioning does not**
832 **impact fear learning. a**. Protocol for optogenetic manipulations during fear conditioning. On Day
833 2, mice received 5 CS-US associations. The US was either optogenetic stimulation alone or
834 optogenetic stimulation plus footshock. **b.** Average freezing levels during the CS-US association
835 of optogenetic stimulation alone. There was no difference in the overall freezing levels for the CS^-
836 and CS^+ between ChR2 and GFP (ns, P = 0.4804, opsin x CS - two-way RM ANOVA, n = 6 GFP,
837 n = 7 ChR2). **c.** During retrieval, there was no effect on freezing upon activation of SST^+ vlPAG
838 cells as an US (ns, P = 0.4804, opsin x CS effect - two-way RM ANOVA, n = 6 GFP, n = 7 ChR2).
839 **d.** Average freezing levels during the CS-US association of optogenetic stimulation plus footshock.
840 There was no difference in the overall freezing levels for the CS^+ and CS^- between ChR2 and GFP

841 (ns, P = 0.8663, opsin x CS effect - two-way RM ANOVA, n = 6 GFP, n = 7 ChR2). **e.** During
842 retrieval, there was no difference in the fear expression by the activation of the SST^+ vlPAG cells
843 (ns, P = 0.8967, opsin x CS effect - two-way RM ANOVA, n = 6 GFP, n = 7 ChR2).

844 **Supplementary Figure 7. Optogenetic effect observed during CFCA is not due to alteration**
845 **of somatostatin levels nor mediated by VIP^+ vlPAG cells. a**. Sst-IRES-Cre heterozygotic mice
846 received a bilateral injection of opsins in the vlPAG, and optic fibers were implanted above the
847 vlPAG. **b.** A representative example of expression patterns of ChR2 within SST^+ vlPAG cells. **c.**
848 Average freezing values during retrieval. ChR2 and GFP groups were pooled together because no
849 differences were found in the conditioning level (data not shown). The average freezing values
850 during CS^+ were higher than CS^- or baseline (BL) periods (****, P < 0.0001, Friedman test, n = 13
851 mice). **d.** Optogenetic activation of SST^+ vlPAG cells abolished the analgesic effect induced by
852 defensive states (**, P = 0.0048, opsin x CS - two-way RM ANOVA, n = 6 GFP, n = 7 ChR2).
853 The mean latency of NC response for the CS^+ was significantly different between the ChR2 and
854 GFP groups (*, P = 0.0300, Bonferroni post-hoc test, n = 6 GFP, n = 7 ChR2). For the ChR2 group,
855 the latency of NC response during CS^+ was equivalent to the CS^- (ns, P = 0.3342, Bonferroni post-
856 hoc test). On the contrary, the latency of NC response between the CSs was different for the GFP
857 group (****, P = 0.0001, Bonferroni post-hoc test). **e.** VIP-IRES-Cre mice received a bilateral
858 injection of opsins in the vlPAG, and optic fibers were implanted above the vlPAG. **f.**
859 Representative example of the expression pattern of ArchT within VIP^+ vlPAG cells. **g.** ArchT and
860 GFP groups were pooled together because no differences were found in the conditioning level (data
861 not shown). The average freezing values during CS^+ were higher than CS^- or BL periods (****, P
862 < 0.0001, one-way RM ANOVA, n = 10 mice). **h.** Optogenetic inhibition of VIP^+ cells did not
863 change the analgesic effect for the ArchT group when compared to the GFP (ns, P = 0.5455, opsin

x CS effect - two-way RM ANOVA, n = 5 GFP, n = 5 ArchT). The latency of NC response was higher for the CS^+ trials compared to the CS^- trials for both GFP and ArchT (***, $P < 0.01$, Bonferroni post-hoc test, n = 5 GFP, n = 5 ArchT).

Supplementary Figure 8. Optogenetic activation of SST^+ vlPAG cells did not affect tactile sensitivity. a. Perievent stimulus time histogram indicating the spiking latency of a purely tactile neuron recorded in the spinal cord in response to gentle brushing of the skin. **b.** Representative spiking activity latency of a purely tactile neuron recorded in the spinal cord in response to gentle brushing of the skin with or without activation of ChR2 expressing SST^+ vlPAG cells. **c.** The activation of ChR2 expressing SST^+ vlPAG cells of tactile neurons recorded in the spinal cord in response to gentle brushing of the skin had no effect on the average firing activity (Paired t-test, P = 0.6929, n = 5 cells).

Supplementary Figure 9. Optogenetic manipulation of GFP expressing vlPAG cells did not affect analgesia. a. Single-unit recordings of WDR cells in the lumbar spinal cord during optogenetic manipulation of GFP expressing SST^+ vlPAG inputs to the RVM. **b**. Photostimulation of SST^+ vlPAG inputs to the RVM has no effect.

Supplementary Figure 10. Optical fiber placement for VIP-Cre. Anatomical location of the tip of the optic fiber for VIP-Cre mice (n = 10).

Supplementary Figure 11. Optical fiber placement for SST-Cre mice. Anatomical location of the tip of the optic fiber for SST-Cre mice (n = 39).

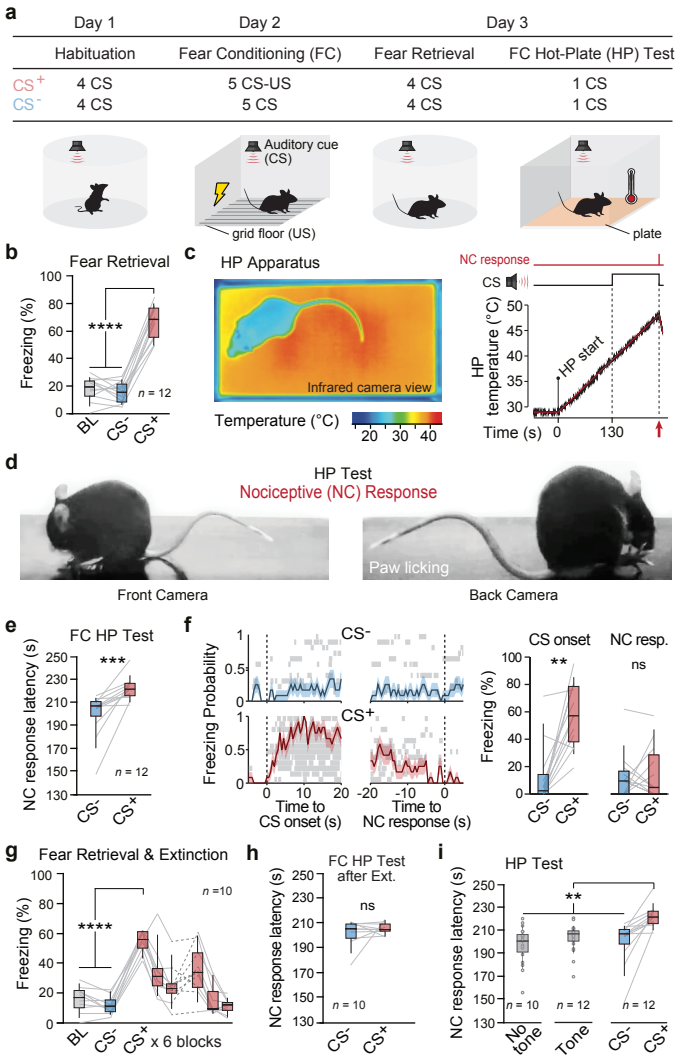

Winke et al., Figure 1

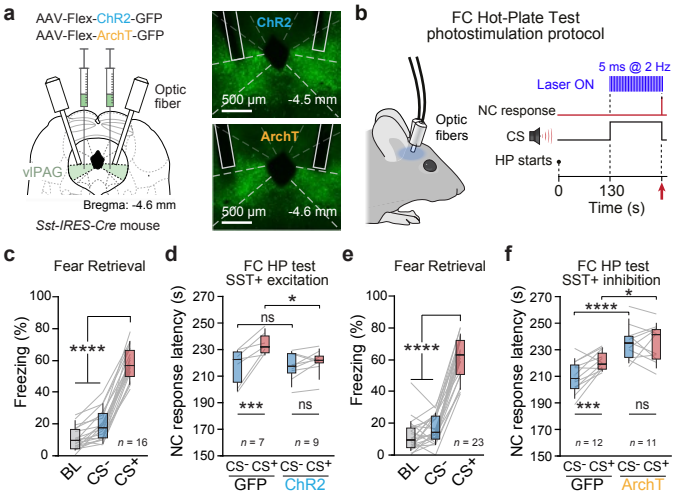

Winke et al., Figure 2

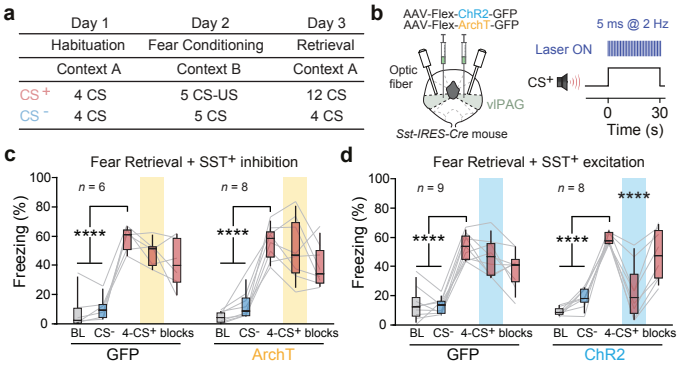

Winke et al., Figure 3

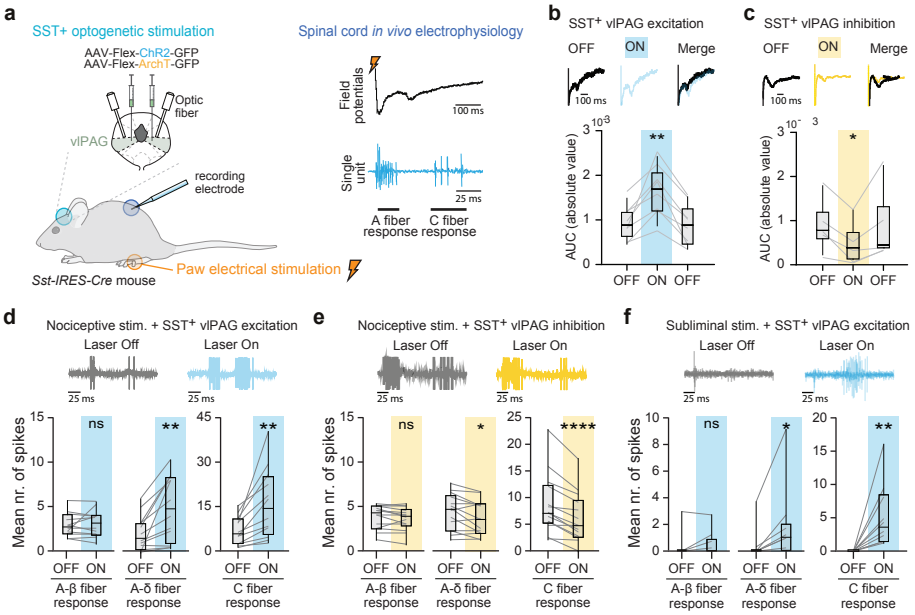

Winke et al, Figure 4

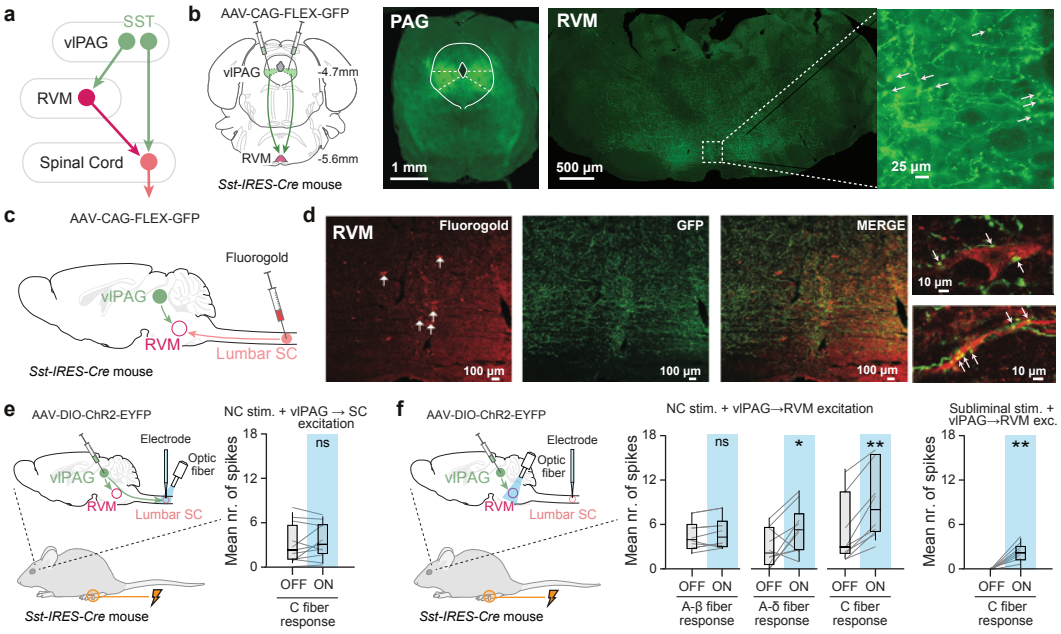

Winke et al., Figure 5

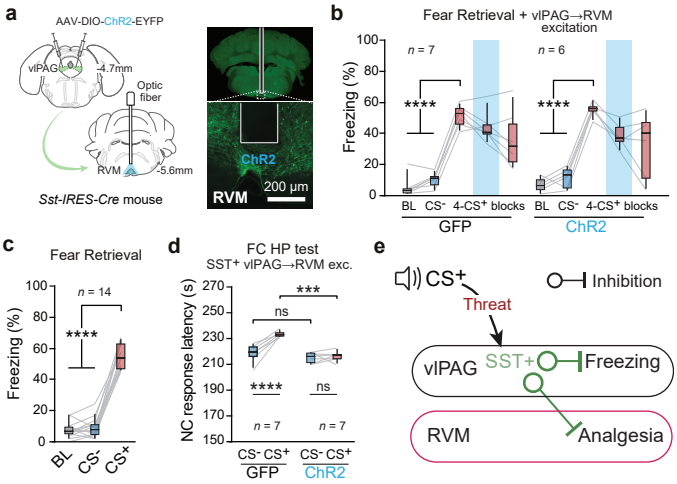

Winke et al., Figure 6

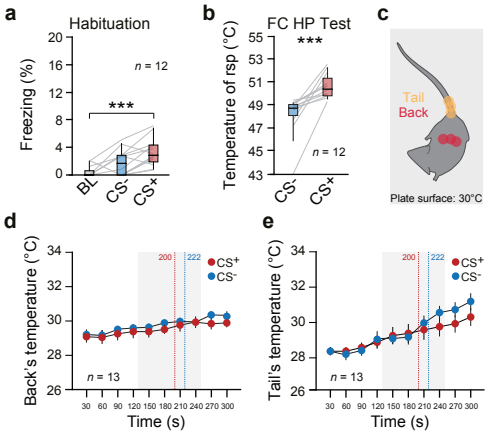

Winke et al., Supplementary Figure 1

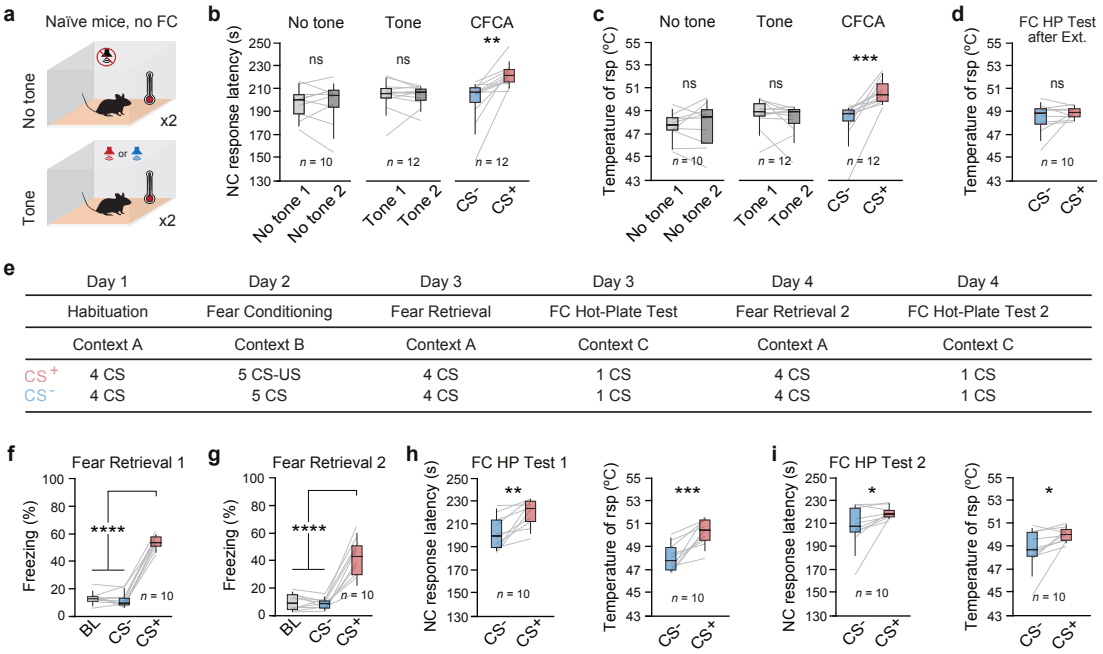

Winke et al., Supplementary Figure 2

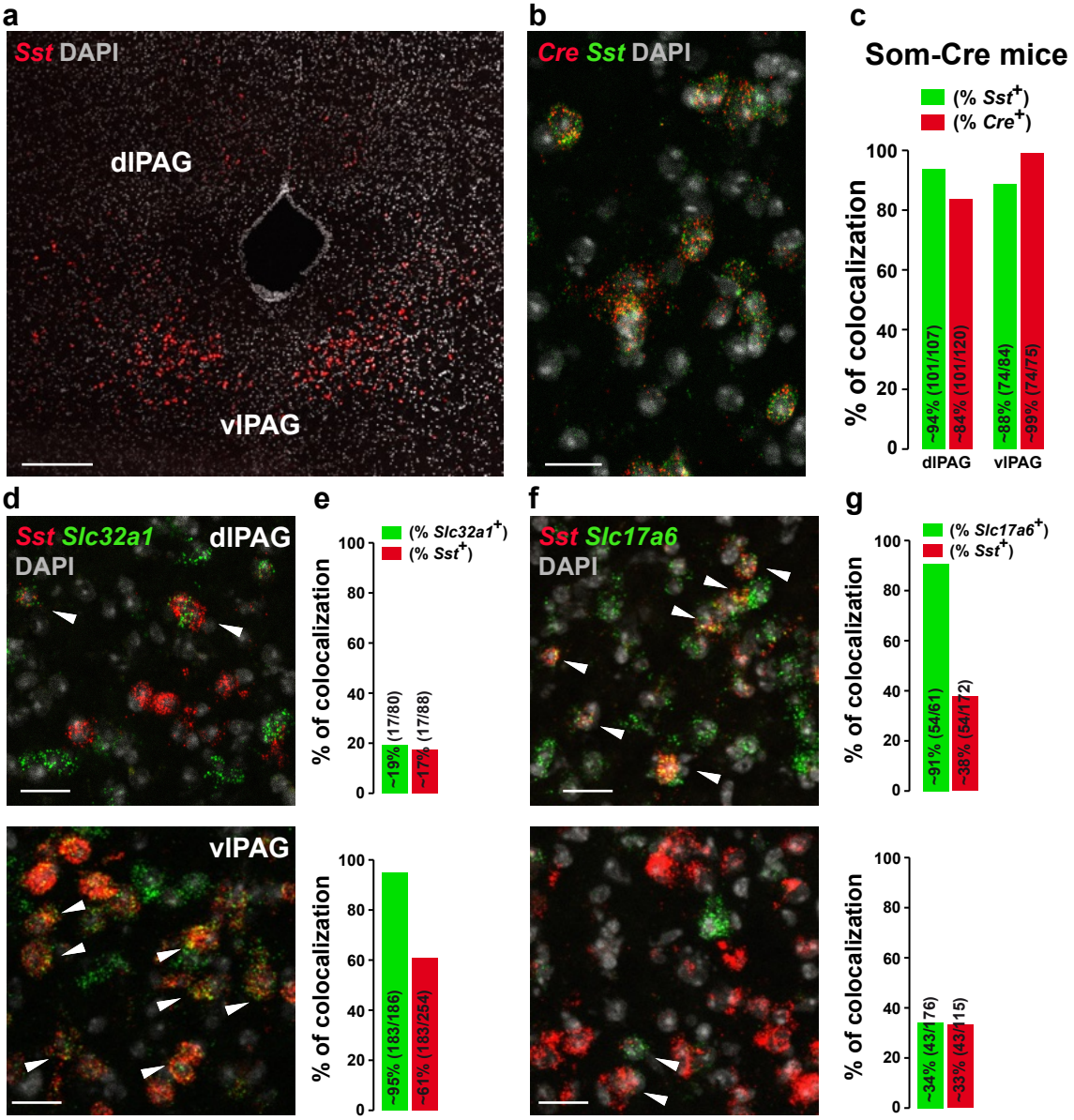

Winke et al., Supplementary Figure 3

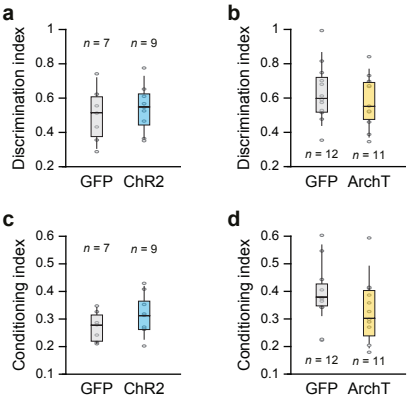

Winke et al., Supplementary Figure 4

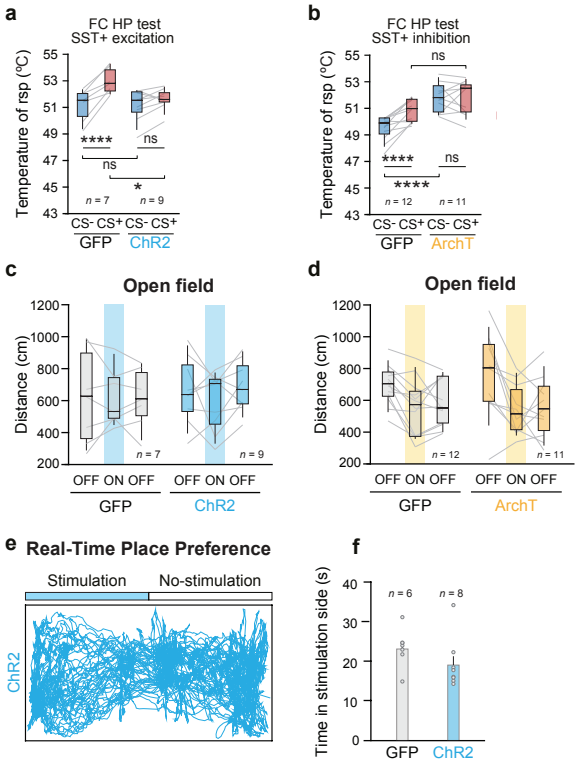

Winke et al., Supplementary Figure 5

a

	Day 1	Day 2	Day 3
	Habituation	Fear Conditioning - Opto stim.	Retrieval
	Context A	Context B	Context A
CS^+	4 CS	5 CS-US	4 CS
CS^-	4 CS	5 CS	4 CS

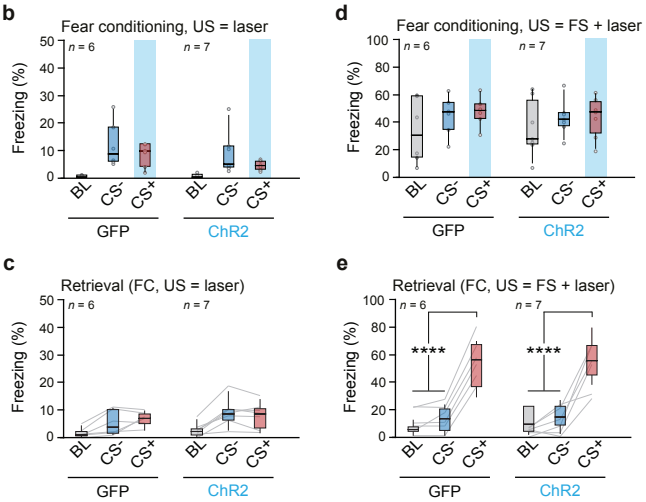

Winke et al., Supplementary Figure 6

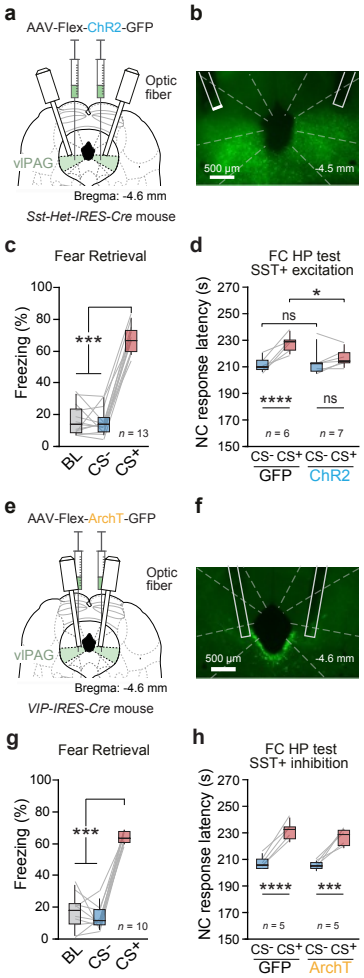

Winke et al., Supplementary Figure 7

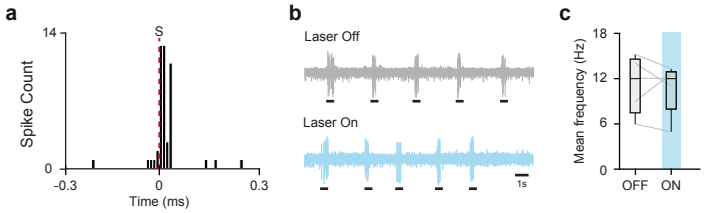

Winke et al., Supplementary Figure 8

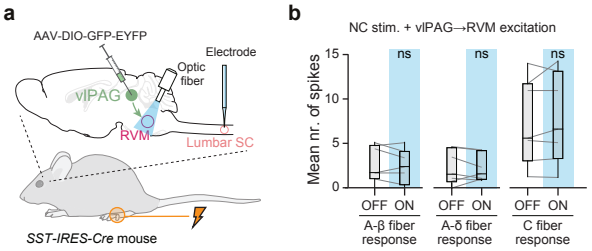

Winke et al., Supplementary Figure 9

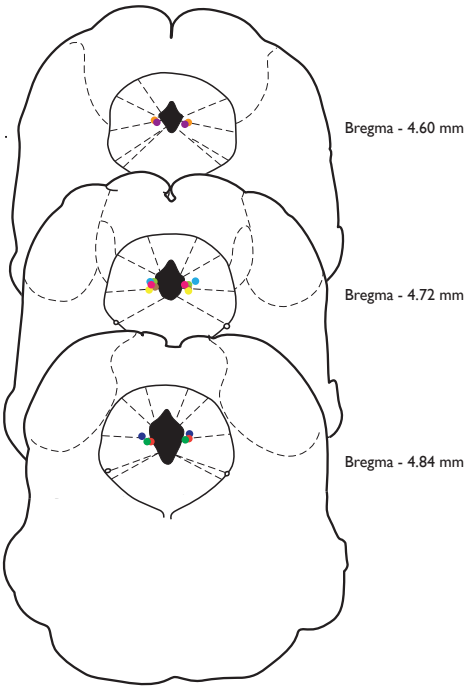

Winke et al, Supplementary Figure 10

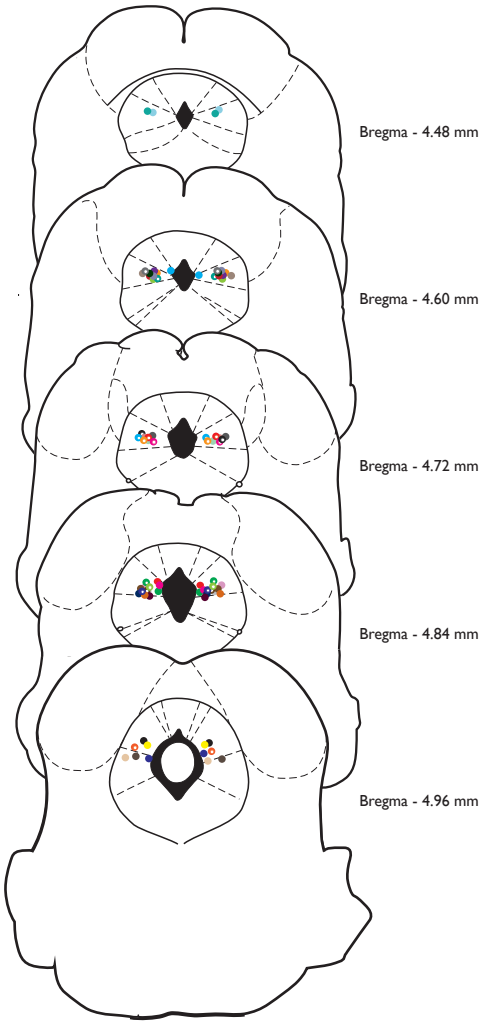

Winke et al, Supplementary Figure 11

Supplementary Table 1 | Summary of statistical results associated with the Figures and Supplementary Figures

Figure number	Normality test	Statistic method	Main effect	Post hoc multiple comparisons test	Number of mice	Number of cells
1b	Passed	One-way RMA NOVA followed by Bonferroni post-hoc test	$F_{(2, 22)} = 160.8$ P value < 0,0001	BL vs. CS^-, P > 0.9999, ns BL vs. CS^+, P < 0,0001 CS^- vs. CS^+, P < 0,0001	12	NA
1e	Failed	Wilcoxon matched-pairs signed rank test (two-tailed)	P = 0.0005	$W = 78.00$	12	NA
1f	Onset, failed Offset, failed	Wilcoxon matched-pairs signed rank test (two-tailed)	Onset, P = 0.0015 Offset, P = 0.8330, ns	Onset, $W = 74$ Offset, $W = 6$	12	NA
1g	Failed	Friedman test followed by Dunn's multiple post-hoc test	P value < 0,0001 $Q = 48.13$	BL vs. CS^-, P > 0.9999, ns BL/CS^- vs. $CS^+_{1st\ block}$, P < 0,0001 CS^- vs. $CS^+_{5th/6th\ block}$, P > 0.9999, ns $CS^+_{1st\ block}$ vs. $CS^+_{5th/6th\ block}$, P < 0.005	10	NA
1h	Passed	Paired t-test (two-tailed)	P = 0.4365, ns	$t_9 = 0.8143$	10	NA
1i	Failed	Krustal-Wallis test followed by Dunn's multiple post-hoc test	P < 0.0001 $H = 25.32$	No tone vs. Tone, P = 0.7710, ns No tone vs. CS^-, P > 0.9999, ns Tone vs. CS^-, P > 0.9999, ns No tone vs. CS^+, P < 0.0001 Tone vs. CS^+, P = 0.0009 CS^- vs CS^+, P = 0.0033	No tone = 10 Tone = 12 CSs =12	NA
2c	Passed	One-way RM ANOVA followed by Bonferroni post-hoc test	$F_{(2,30)} = 396.8$ P < 0.0001	BL vs. CS^-, P > 0.9999, ns BL vs. CS^+, P < 0,0001 CS^- vs. CS^+, P < 0,0001	16	NA
2d	Passed	Two-way RM ANOVA followed by Bonferroni post-hoc test	Opsin x CS, $F_{(1,14)} = 8.514$ P = 0.0112	CS^- vs. CS^+, GFP, P = 0.0003 CS^- vs. CS^+, ChR2, P = 0.3876, ns GFP vs. ChR2, CS^-, P > 0.9999, ns GFP vs. ChR2, CS^+, P = 0.0344	GFP = 7 ChR2 = 9	NA
2e	Passed	One-way RM ANOVA followed by Bonferroni post-hoc test	$F_{(2,44)} = 280.4$ P < 0.0001	BL vs. CS^-, P = 0.2337, ns BL vs. CS^+, P < 0,0001 CS^- vs. CS^+, P < 0,0001	23	NA
2f	Passed	Two-way RM ANOVA followed by Bonferroni post-hoc test	Opsin x CS, $F_{(1,21)} = 10.64$ P = 0.0037	CS^- vs. CS^+, GFP, P = 0.0003 CS^- vs. CS^+, ArchT, P > 0.9999, ns GFP vs. ArchT, CS^-, P < 0,0001 GFP vs. ArchT, CS^+, P = 0.0265	GFP = 12 ArchT = 11	NA

NA = Not applicable **NS = Not significant** **Supp = Supplementary figure**

Supplementary Table 1 | Summary of statistical results associated with the Figures and Supplementary Figures

3c	Passed	Two-way RM ANOVA followed by Bonferroni post-hoc test	Opsin x CS, $F_{(4,48)} = 0.1954$ P = 0.9396, ns	BL vs. CS^-, GFP/ArchT, P > 0.9999, ns BL vs. $CS^+_{1st/2nd/3rd}$, GFP/ArchT, P < 0,0001 CS^- vs. $CS^+_{1st/2nd/3rd}$, GFP/ArchT, P < 0,0001 CS^+_{1st} vs. $CS^+_{2nd/3rd}$, GFP/ArchT, P > 0.9999, ns CS^+_{2nd} vs. CS^+_{3rd}, GFP/ArchT, P > 0.9999, ns GFP vs. ArchT, BL/CS^-/$CS^+_{1st/2nd/3rd}$, P > 0.9999, ns	GFP = 6 ArchT = 8	NA
3d	Passed	Two-way RM ANOVA followed by Bonferroni post-hoc test	Opsin x CS, $F_{(4,60)} = 7.957$ P < 0.0001	BL vs. CS^-, GFP/ChR2, P > 0.9999, ns BL vs. $CS^+_{1st/2nd/3rd}$, GFP, P < 0,0001 CS^- vs. $CS^+_{1st/2nd/3rd}$, GFP, P < 0,0001 CS^+_{1st} vs. $CS^+_{2nd/3rd,}$ GFP, P > 0.9999, ns CS^+_{2nd} vs. $CS^+_{3rd,}$ GFP, P > 0.9999, ns BL vs. $CS^+_{1st/3rd}$, ChR2, P < 0,0001 BL vs. CS^+_{2nd}, ChR2, P = 0.0789, ns CS^- vs. $CS^+_{1st/3rd}$, ChR2, P < 0,0001 CS^- vs. CS^+_{2nd}, ChR2, P > 0.9999, ns CS^+_{1st} vs. CS^+_{2nd}, ChR2, P < 0,0001 CS^+_{1st} vs. CS^+_{3rd}, ChR2, P = 0.2372, ns CS^+_{2nd} vs. CS^+_{3rd}, ChR2, P < 0,0001 GFP vs. ChR2, BL/CS-/$CS^+_{1st/3rd}$, P > 0.9999, ns GFP vs. ChR2, $CS^+_{2nd,}$ P = 0.0002	GFP = 9 ChR2 = 8	NA
4b	Passed	One-way RM ANOVA followed by Bonferroni post-hoc test	$F_{(2, 14)} = 17{,}94$ P = 0,0001	OFF1 vs. ON, P = 0.0006 OFF2 vs. ON, P = 0.0003 OFF1 vs. OFF2, P > 0.9999, ns	8	NA
4c	Passed	One-way RM ANOVA followed by Bonferroni post-hoc test	$F_{(2, 8)} = 5{,}826$ P = 0,0275	OFF1 vs. ON, P = 0.0414 OFF2 vs. ON, P = 0.0452 OFF1 vs. OFF2, P = 0.9980, ns	5	NA
4d	A-β fiber, passed A-δ fiber, passed C fiber, passed	Paired t-test (two-tailed)	A-β fiber, P = 0.5430, ns A-δ fiber, P = 0.0022 C fiber, P = 0.0033	A-β fiber, $t_{11} = 0.6319$ A-δ fiber, $t_{11} = 3.959$ C fiber, $t_{11} = 3.739$	8	A-β fiber,11 A-δ fiber, 11 C fiber, 11
4e	A-β fiber, passed A-δ fiber, passed C fiber, passed	Paired t-test (two-tailed)	A-β fiber, P = 0.1386, ns A-δ fiber, P = 0.0241 C fiber, P < 0.0001	A-β fiber, $t_{13} = 1.578$ A-β fiber, $t_{13} = 2.553$ C fiber, $t_{13} = 6.274$	5	A-β fiber,14 A-δ fiber, 14 C fiber, 14
4f	A-β fiber, failed A-δ fiber, failed C fiber, failed	Wilcoxon matched-pairs signed rank test (two-tailed)	A-β fiber, P = 0.3750, ns A-δ fiber, P = 0.0156 C fiber, P = 0.0020	A-β fiber, $W = 7.0$ A-β fiber, $W = 28.0$ C fiber, $W = 55.0$	8	A-β fiber,10 A-δ fiber, 10 C fiber, 10
5e	Passed	Paired t-test (two-tailed)	P = 0.3683, ns	$t_{10} = 0.94222$	7	11

NA = Not applicable **NS = Not significant** **Supp = Supplementary figure**

Supplementary Table 1 | Summary of statistical results associated with the Figures and Supplementary Figures

5f, left	A-β fiber, passed A-δ fiber, passed C fiber, failed	Paired t-test (two-tailed) Paired t-test (two-tailed) Wilcoxon matched-pairs signed rank test (two-tailed)	A-β fiber, P = 0.0740, ns A-δ fiber, P = 0.0346 C fiber, P = 0.0020	A- β fiber, t_9 = 2.021 A-δ fiber, t_9 = 2.487 C fiber, *W* = 55.0	7	A-β fiber,10 A-δ fiber, 10 C fiber, 10
5f, right	Failed	Wilcoxon matched-pairs signed rank test (two-tailed)	P = 0.0078	*W* = 36.0	7	9
6b	Passed	Two-way RM ANOVA followed by Bonferroni post-hoc test	Opsin x CS, $F_{(4,44)}$ = 0.6292 P = 0.6443, ns	BL vs. CS^{-}, GFP/ChR2, P > 0.9999, ns BL vs. $CS^{+}_{1st/2nd/3rd}$, GFP/ChR2, P < 0,0001 CS^{-} vs. $CS^{+}_{1st/2nd/3rd}$, GFP/ChR2, P < 0,0001 CS^{+}_{1st} vs. CS^{+}_{2nd}, GFP/ChR2, P > 0.9999, ns CS^{+}_{2nd} vs. CS^{+}_{3rd}, GFP/ChR2, P > 0.9999, ns CS^{+}_{1st} vs. CS^{+}_{3rd}, GFP, P = 0.0090 CS^{+}_{1st} vs. CS^{+}_{3rd}, ChR2, P = 0.0003 GFP vs. ChR2, BL/CS^{-}/$CS^{+}_{1st/2nd/3rd}$, P > 0.9999, ns	GFP = 7 ChR2 = 6	NA
6c	Passed	One-way RM ANOVA followed by Bonferroni post-hoc test	$F_{(2,26)}$ = 274.2 P < 0.0001	BL vs. CS^{-}, P > 0.9999, ns BL vs. CS^{+}, P < 0,0001 CS^{-} vs. CS^{+}, P < 0,0001	14	NA
6d	Passed	Two-way RM ANOVA followed by Bonferroni post-hoc test	Opsin x CS, $F_{(1,12)}$ = 10.91 P = 0.0063	CS^{-} vs. CS^{+} - GFP, P < 0,0001 CS^{-} vs. CS^{+} - ChR2, P > 0.9999, ns GFP vs. ChR2 – CS^{-}, P = 0.5378, ns GFP vs. ChR2 – CS^{+}, P = 0.0002	GFP = 7 ChR2 = 7	NA
Supp1a	Failed	Friedman test followed by Dunn's multiple post-hoc test	P = 0.0003 *Q* = 16.55	BL vs. CS^{-}, P = 0.3074, ns BL vs. CS^{+}, P = 0.0003 CS^{-} vs. CS^{+}, P = 0.0742, ns	12	NA
Supp1b	Failed	Wilcoxon matched-pairs signed rank test (two-tailed)	P = 0.0005	*W* = 78.0	12	NA
Supp1d	Passed	Mixed-effects model followed by Bonferroni post-hoc test	CS x Time, $F_{(9,238)}$ = 0.1716 P = 0.9967	CS^{+} vs. CS^{-} for each time point, all P > 0.9999, ns	13	NA
Supp1e	Passed	Mixed-effects model followed by Bonferroni post-hoc test	CS x Time, $F_{(9,238)}$ = 0.7147 P = 0.6952	CS^{+} vs. CS^{-} for each time point, all P > 0.9999, ns	13	NA
Supp2b	No tone, passed Tone, passed CFCA, failed	Paired t-test (two-tailed) Paired t-test (two-tailed) Wilcoxon matched-pairs signed rank test (two-tailed)	No tone, P = 0.9866, ns Tone, P = 0.9085, ns CFCA, P = 0.0005	No tone, t_9 = 0.01732 Tone, t_{11} = 0.1176 CFCA, *W* = 78.0	No tone= 10 Tone = 12 CFCA =12	NA

NA = Not applicable **NS = Not significant** **Supp = Supplementary figure**

Supplementary Table 1 | Summary of statistical results associated with the Figures and Supplementary Figures

Supp2b	Failed	Krustal-Wallis test followed by Dunn's multiple post-hoc test	P = 0.0001 *H* = 25.45	No tone 1 vs. No tone 2/Tone 1/Tone 2/CS-, P > 0.9999, ns No tone 2 vs. Tone 1/Tone 2/CS-, P > 0.9999, ns Tone 1 vs. Tone 2/CS-, P > 0.9999, ns Tone 2 vs. Tone CS-, P > 0.9999, ns No tone 1 vs. CS+, P = 0.0002 No tone 2 vs. CS+, P = 0.0009 Tone 1 vs. CS+, P = 0.0178 Tone 2 vs. CS+, P = 0.0133 CS- vs. CS+, P =0.0082	No tone = 10 Tone = 12 CFCA =12	NA
Supp2c	No tone, passed Tone, failed CFCA, failed	Paired t-test (two-tailed) Wilcoxon matched-pairs signed rank test (two-tailed)	No tone, P = 0.6216, ns Tone, P = 0.4375, ns CS, P = 0.0005	No tone, t_9 = 0.5111 Tone, *W* = -21.0 CFCA, *W* = 78.0	No tone = 10 Tone = 12 CFCA =12	NA
Supp2c	Failed	Krustal-Wallis test followed by Dunn's multiple post-hoc test	P < 0.0001 *H* = 29.30	No tone 1 vs. No tone 2/Tone 1/Tone 2/CS^-, P > 0.9999, ns No tone 2 vs. Tone 1/Tone 2/CS^-, P > 0.9999, ns Tone 1 vs. Tone 2/CS-, P > 0.9999, ns Tone 2 vs. Tone CS^-, P > 0.9999, ns No tone 1 vs. CS^+, P < 0.0001 No tone 2 vs. CS^+, P = 0.0010 Tone 1 vs. CS^+, P = 0.0339 Tone 2 vs. CS^+, P = 0.0037 CS^- vs. CS^+, P =0.0033	No tone = 10 Tone = 12 CFCA =12	NA
Supp2d	Passed	Paired t-test (two-tailed)	P = 0.3276, ns	t_9 = 1.035	10	NA
Supp2f	Passed	One-way RM ANOVA followed by Bonferroni post-hoc test	$F_{(2,18)}$ = 558.2 P < 0.0001	BL vs. CS^-, P > 0.9999, ns BL vs. CS^+, P < 0,0001 CS^- vs. CS^+, P < 0,0001	10	NA
Supp2g	Passed	One-way RM ANOVA followed by Bonferroni post-hoc test	$F_{(2,18)}$ = 56.00 P < 0.0001	BL vs. CS^-, P > 0.9999, ns BL vs. CS^+, P < 0,0001 CS^- vs. CS^+, P < 0,0001	10	NA
Supp2h, left	Passed	Paired t-test (two-tailed)	P = 0.0029	t_9 = 4.054	10	NA
Supp2h, right	Passed	Paired t-test (two-tailed)	P = 0.0006	t_9 = 5.184	10	NA
Supp2i, left	Passed	Paired t-test (two-tailed)	P = 0.0362	t_9 = 2.459	10	NA

NA = Not applicable **NS = Not significant** **Supp = Supplementary figure**

Supplementary Table 1 | Summary of statistical results associated with the Figures and Supplementary Figures

Supp2i, right	Passed	Paired t-test (two-tailed)	P = 0.0245	$t_9 = 2.697$	10	NA
Supp4a	Passed	Unpaired t-test (two-tailed)	P = 0.6052	$t_{14} = 0.5288$	GFP = 7 ChR2 = 9	NA
Supp4b	Passed	Unpaired t-test (two-tailed)	P = 0.4575	$t_{21} = 0.7569$	GFP = 12 ArchT = 11	NA
Supp4c	Passed	Unpaired t-test (two-tailed)	P = 0.2333	$t_{14} = 1.246$	GFP = 7 ChR2 = 9	NA
Supp4d	Passed	Unpaired t-test (two-tailed)	P = 0.1320	$t_{21} = 1.567$	GFP = 12 ArchT = 11	NA
Supp5a	Passed	Two-way RM ANOVA followed by Bonferroni post-hoc test	Opsin x CS, $F_{(1,14)} = 11.40$ P = 0.0045	CS^- vs. CS^+, GFP, P < 0,0001 CS^- vs. CS^+, ChR2, P = 0.1783, ns GFP vs. ChR2, CS^-, P > 0.9999, ns GFP vs. ChR2, CS^+, P = 0.0322	GFP = 7 ChR2 = 9	NA
Supp5b	Passed	Two-way RM ANOVA followed by Bonferroni post-hoc test	Opsin x CS, $F_{(1,21)} = 10.84$ P = 0.0035	CS^- vs. CS^+, GFP, P = 0.0003 CS^- vs. CS^+, ArchT, P > 0.9999, ns GFP vs. ArchT, CS^-, P < 0,0001 GFP vs. ArchT, CS^+, P = 0.0704, ns	GFP = 12 ArchT = 11	NA
Supp5c	Passed	Two-way RM ANOVA followed by Bonferroni post-hoc test	Opsin x Light, $F_{(2,28)} = 0.6855$ P = 0.5121, ns	OFF_1 vs. ON, GFP/ChR2, P > 0.9999, ns OFF_2 vs. ON, GFP/ChR2, P > 0.9999, ns OFF_1 vs. OFF_2, GFP/ChR2, P > 0.9999, ns GFP vs. ChR2, OFF_1/ON/OFF_2, P > 0.9999, ns	GFP = 7 ChR2 = 9	NA
Supp5d	Passed	Two-way RM ANOVA followed by Bonferroni post-hoc test	Opsin x Light, $F_{(2,42)} = 0.9243$ P = 0.4047, ns	OFF_1 vs. ON, GFP, P = 0.0165 OFF_1 vs. ON, ArchT, P = 0.0003 OFF_2 vs. ON, GFP/ArchT P > 0.9999, ns OFF_1 vs. OFF_2, GFP/ArchT, P > 0.9999, ns GFP vs. ArchT, OFF_1/ON/OFF_2, P > 0.9999, ns	GFP = 12 ArchT = 11	NA
Supp5f	Failed	Mann Whitney test (two-tailed)	P = 0.1812	$U = 13$	GFP = 6 ChR2 = 8	NA
Supp6b	Passed	Two-way RM ANOVA followed by Bonferroni post-hoc test	Opsin x CS, $F_{(2,22)} = 0.7582$ P = 0.4804, ns	GFP vs. ChR2, BL/CS^-/CS^+, P > 0.9999, ns	GFP = 6 ChR2 = 7	NA
Supp6c	Passed	Two-way RM ANOVA followed by Bonferroni post-hoc test	Opsin x CS, $F_{(2,22)} = 1.926$ P = 0.1695, ns	GFP vs. ChR2, BL/CS_-/CS_+, P > 0.9999, ns	GFP = 6 ChR2 = 7	NA

NA = Not applicable **NS = Not significant** **Supp = Supplementary figure**

Supplementary Table 1 | Summary of statistical results associated with the Figures and Supplementary Figures

Supp6d	Passed	Two-way RM ANOVA followed by Bonferroni post-hoc test	Opsin x CS, $F_{(2,22)} = 0.1444$ P = 0.8663, ns	GFP vs. ChR2, BL/CS^-/CS^+, P > 0.9999, ns	GFP = 6 ChR2 = 7	NA
Supp6e	Passed	Two-way RM ANOVA followed by Bonferroni post-hoc test	Opsin x CS, $F_{(2,22)} = 0.1095$ P = 0.8967, ns	GFP vs. ChR2, BL/CS^-/CS^+, P > 0.9999, ns BL vs. CS^-, GFP, P > 0.9999, ns BL vs. CS^-, ChR2, P > 0.5328, ns BL vs. CS^+, GFP/ChR2, P < 0,0001 CS^- vs. CS^+, GFP/ChR2, P < 0,0001	GFP = 6 ChR2 = 7	NA
Supp7c	Failed	Friedman test followed by Dunn's multiple post-hoc test	P value < 0.0001 $Q = 19.85$	BL vs. CS^-, P > 0.9999, ns BL vs. CS^+, P = 0,0012 CS^- vs. CS^+, P = 0,0001	13	NA
Supp7d	Passed	Two-way RM ANOVA followed by Bonferroni post-hoc test	Opsin x CS, $F_{(1,11)} = 12.39$ P = 0.0048	CS^- vs. CS^+, GFP, P = 0.0001 CS^- vs. CS^+, ChR2, P = 0.3342, ns GFP vs. ChR2, CS^-, P > 0.9999, ns GFP vs. ChR2, CS^+, P = 0.0300	GFP = 6 ChR2 = 7	NA
Supp7g	Passed	One-way RM ANOVA followed by Bonferroni post-hoc test	$F_{(2,18)} = 147.1$ P < 0.0001	BL vs. CS^-, P = 0.8655, ns BL vs. CS^+, P < 0,0001 CS^- vs. CS^+, P < 0,0001	10	NA
Supp7h	Passed	Two-way RM ANOVA followed by Bonferroni post-hoc test	Opsin x CS, $F_{(1,8)} = 0.3984$ P = 0.5455, ns	CS^- vs. CS^+, GFP, P = 0.0001 CS^- vs. CS^+, ArchT, P = 0.0003 GFP vs. ChR2, CS^-, P > 0.9999, ns GFP vs. ChR2, CS^+, P = 0.3869, ns	GFP = 5 ArchT = 5	NA
Supp8c	Passed	Paired t-test (two-tailed)	P = 0.6929, ns	$t_4 = 0.4247$	5	5
Supp9b	A-β fiber, passed A-δ fiber, passed C fiber, passed	Paired t-test (two-tailed)	A-β fiber, P = 0.3750, ns A-δ fiber, P = 0.7369, ns C fiber, P = 0.4150, ns	A- β fiber, $t_6 = 0.9564$ A-δ fiber, $t_6 = 0.3520$ C fiber, $t_6 = 0.8755$	3	A-β fiber, 7 A-δ fiber, 7 C fiber, 7

NA = Not applicable **NS = Not significant** **Supp = Supplementary figure**